CHARACTERIZING AQUITARD PROPERTIES FROM THE RESPONSE OF GROUTED VIBRATING WIRE PIEZOMETERS TO SURFACE LOADING

A Thesis submitted to the College of

Graduate and Postdoctoral Studies

In Partial Fulfillment of the Requirements

For the Degree of Master of Science

In the Department of Civil, Geological, and Environmental Engineering

University of Saskatchewan

Saskatoon

By

CHARLES NATHAN DOURADO

PERMISSION TO USE

In presenting this thesis/dissertation in partial fulfillment of the requirements for a Postgraduate degree from the University of Saskatchewan, I agree that the Libraries of this University may make it freely available for inspection. I further agree that permission for copying of this thesis/dissertation in any manner, in whole or in part, for scholarly purposes may be granted by the professor or professors who supervised my thesis/dissertation work or, in their absence, by the Head of the Department or the Dean of the College in which my thesis work was done. It is understood that any copying or publication or use of this thesis/dissertation or parts thereof for financial gain shall not be allowed without my written permission. It is also understood that due recognition shall be given to me and to the University of Saskatchewan in any scholarly use which may be made of any material in my thesis/dissertation.

Requests for permission to copy or to make other uses of materials in this thesis/dissertation in whole or part should be addressed to:

Head of the Department of Civil, Geological, and Environmental Engineering
University of Saskatchewan
Saskatoon, Saskatchewan S7N 5A9
Canada

OR

Dean
College of Graduate and Postdoctoral Studies
University of Saskatchewan
116 Thorvaldson Building, 110 Science Place
Saskatoon, Saskatchewan S7N 5C9
Canada

ABSTRACT

Barometric Response Functions (BRF) are used to characterize the observed pore pressure response within grouted-in vibrating wire piezometers to changes in surface barometric pressure. The BRF facilitates determination of loading efficiency (λ_{LE}) which is a function of *in situ* compressibility. However, the mechanisms which control the characteristic shape of a BRF within a fully grouted borehole are not well understood. In this study, the transient pore pressure responses to both local instantaneous loading and transient barometric loading are used to improve our understanding of the BRF response.

Two boreholes were each drilled to a depth of 200 m in a thick clay sequence in Southern Saskatchewan. One borehole was advanced through continuous coring while the other was drilled using rotary fluid circulation. Ten vibrating-wire piezometers (VWPs) were placed within each borehole at a 10m spacing. The pore pressure in all VWPs and barometric pressure was recorded concurrently for 3 years following installation. Multiple-linear regression was undertaken on both data sets to determine the BRF for each VWP. In addition, localized instantaneous surface loading was applied using heavy construction equipment. The coupled load-pore responses were simulated using a commercial coupled stress and water flow finite element model to evaluate the grout and formation hydraulic and mechanical properties.

The BRF characteristics of the monitored depth profile were used to identify the limitations of linear-regression methods for determining λ_{LE}. Near-borehole influences, such as stress-release induced damage or mud filter-cake build-up, can influence the magnitude and timing of observed pore pressures. These limitations can be addressed by judicious selection of drilling methods, grouting procedures, and pressure sensor resolution. In addition, a more rigorous interpretation of the BRF can be used to obtain additional information about the *in situ* hydraulic and geomechanical properties of the aquitard. The rigorous analysis of measured pore pressure response to changes in external stress improves our understanding of *in situ* properties and the behavior of low-hydraulic conductivity and low-compressibility formations.

ACKNOWLEDGEMENTS

I feel obligated to acknowledge everyone who contributed to the development of this thesis. Unfortunately, the recommended word count is limited to only 250.

I would like to thank the members of my advisory committee. Lee Barbour and Jim Hendry, we communicated less than was imagined two-and-a-bit-years ago. However, I ruminated on, and feel blessed, for every drop of wisdom you shared. Dave Elwood. Our conversations always run too long, and know no boundaries. Everything you said is a massive part of my education. Although not a committee member, I am grateful for Laura Smith, an assigned mentor and chosen friend. My research site and topic was her metaphorical baby. From the beginning, you shared knowledge, guidance, and physical-help in the field.

I acknowledge the University of Saskatchewan, its abundance of elm trees, and financial support to pursue my studies. My stipend ultimately derived from Lee's Industrial Research Chair. This was supplemented by departmental graduate scholarships and the tortured pleasure of being a teaching assistant.

I am forever indebted to my family for their support. My parents, Hyacinth and Manuel Dourado who taught unrelenting patience and kindness. My twin brother, Nicholas Dourado, for the strength and passion to forge an inspiring trail in both academics and arts.

I must thank all graduate students with whom I struggle alongside. Special thanks to James Tipman; without his conversation I may still be looking down an anisotropic rabbit hole.

My dear friends and fellow bunny-thugs, who truly taught me it's not about attainment, but rather the pursuit of excellence. I could name names, but if you're reading this, you know who you are. To Whom It May Concern, sorry for breaking the recommended word count. Thank you.

TABLE OF CONTENTS

LIST OF TABLES

LIST OF FIGURES

1.0 INTRODUCTION

1.1 Background

The principle formations associated with groundwater flow systems are aquifers and aquitards. The former is defined as a geologic unit that has properties that facilitate the economic extraction of water for some end use. Aquifers have been the primary focus of conventional hydrogeology while research on aquitards has become the focus of more recent studies. These studies have sought to characterize aquitards as regional barriers to flow and often with a view to utilizing these geologic units for the storage of hazardous waste. In general, the methods used to characterize aquifers cannot be applied to aquitards due to their low-permeability (Neuzil, 1986). Fortunately, learnings from geotechnical engineering and novel hydrogeological techniques can be leveraged to improve our understanding of aquitard systems.

Grouted-in vibrating wire piezometers are a useful tool for characterizing hydrogeological conditions. They provide a measurement of pore water pressure (and hence hydraulic head) at a discrete depth. In addition, they exhibit a minimal time to equilibrate with formation pressures and are therefore useful for tracking changes in pore pressure within low-permeability formations. One mechanism which can influence the pore pressure within an aquitard is the load response of the aquitard to continually fluctuating atmospheric pressure.

The compressibility, and subsequently specific storage, of a thick aquitard sequence, can be inferred by determining its loading efficiency (λ_{LE}) (Smith et al., 2013). The λ_{LE} is a linear relationship between the change in barometric pressure and formation pore pressure. The time-dependent response of the monitored pore pressure in response to changes in atmospheric and the concomitant formation pore pressures can be characterized using a barometric response function (BRF). The BRF provides an improved method of estimating λ_{LE} in situations in which the time lag is long and can also be used to identify site hydrogeological conditions such as the degree of confinement (Butler et al., 2011).

BRFs have been analyzed to determine the hydraulic diffusivity of a confined aquifer system (Butler et al., 2011). To the author's knowledge, the mechanisms which control the instantaneous pressure response of a BRF for a confined aquifer, or aquitard, have not been

previously studied. This research intends to study the mechanisms which control the characteristic shape of a BRF for a grouted borehole within a low-permeability formation.

1.2 Objectives

The goal of this work is to improve our understanding of the mechanisms which control the pore pressure response of vibrating wire piezometers within fully-grouted boreholes to surface loading. The hypothesis is that geomechanical and hydraulic properties can be determined by analyzing the changes in formation pore pressure in response to changes in surface loading. This surface loading is generally the result of changes in barometric pressure but in the case of this study also included localized loading using heavy construction equipment.

The specific objectives of this study were to:

1) Identify *in situ* depth-profiles of loading efficiency as well as the instantaneous change in observed pore pressure and transient time-lags within the VWPS in response to atmospheric or localized loading;
2) Characterize the small-strain geomechanical moduli of the grout used to backfill VWPs;
3) Compare the observed pressure response from both atmospheric loading and heavy equipment point loading;
4) Characterize the hydraulic conductivity and compressibility of the surrounding aquitard.

The tasks required to meet the stated objectives were to:

1) Define BRFs for VWPs installed in deep boreholes
2) Conduct laboratory testing on grout samples. An estimate of grout properties is necessary for numerical modelling of deformation and flow resultant from surficial loading;
3) Conduct an experiment to observe the pressure response from heavy equipment point loading;
4) Interpret the VWP responses to surface loading using numerical modelling to define the geomechanical and hydraulic controls on the pore pressure response of grouted-in vibrating wire piezometers.

2.0 LITERATURE REVIEW

2.1 Overview

The three key areas of literature pertinent to the objectives of this study include the following:

- The theoretical relationships that link loading – particularly surface loading – on the pore pressure response within low permeability formations.
- The field approaches that have been used to measure these pore pressure responses
- And finally, the analytical approaches that have been used to estimate *in situ* aquitard properties based on this field monitoring.

2.2 Theoretical Background of Porous Media

The theoretical underpinnings of the coupled (loading and pore pressure) response of a saturated porous media to loading have been extensively studied (Biot, 1941; Nur & Byerlee, 1971; Rice, James R.; Cleary, 1976; Terzaghi, 1927; van der Kamp & Gale, 1983). A saturated porous media like soil is composed of two main components: solid grains which form a skeleton, and voids filled with fluid. Loads applied to the porous media are supported by both the soil-skeleton and pore-fluid, depending on the relative stiffness of these phases. Mathematical relationships can be used to calculate the behaviour of soil when subject to applied changes in total stress or pore pressure, such as occur from civil construction or water withdrawal, respectively.

From a hydrogeological context, water flow and soil volume change (i.e. deformation) are described by the groundwater flow equation:

$$K\nabla^2 h = S_s \frac{dh}{dt} \tag{2-1}$$

$$S_s = \rho g(n\beta_w + m_v) \tag{2-2}$$

where K is the hydraulic conductivity (m/s), h is hydraulic head (m), S_s is specific storage (m^{-1}), ρg is the unit weight of water ($kg \cdot m^{-2} \cdot s^{-1}$), n is the effective porosity (dimensionless), β_w is the bulk compressibility of water (kPa^{-1}), and m_v is the drained one,-dimensional compressibility of

the soil skeleton (kPa^{-1}). The hydraulic head is a summation of pressure head and elevation head. This paper focuses on increments of hydraulic head at a fixed elevation. Therefore the dependent variable of the flow equation will be further discussed as pore-water pressure (p, kPa^{-1})

The flow equation is useful in typical hydrogeology investigations of aquifers. However, applying the flow equation to aquitards is met with obstacles. The equation was derived from principles of both conservation of mass and Darcy's Law. Both are applicable for aquitards unless chemical driving factors are prevalent (Neuzil, 1986). Due to three-dimensional deformation, pumping semi-confined aquifers can immediately influence aquitard hydraulic head (Hsieh, 1996). Therefore, the study of aquitards requires proper consideration of deformation. Two common assumptions inherent within the formulation of specific storage are lateral deformations are negligible and compressibility is constant. It is prudent to be aware of these assumptions when applying analytical, mathematical, or numerical models to interpret and predict groundwater behaviour.

The specific storage describes the volume of water released from storage as a result of changes in water pressure. Including one dimensional compressibility (m_v in Eq. 2.2) assumes that the soil is prevented from deforming laterally during changes in pore pressure. This assumption is valid for most hydrogeological applications since changes in the hydraulic head are relatively slow, and natural hydraulic gradients are low. However, in the prediction of subsidence, lateral deformations may not be adequately calculated, which could have implications for groundwater well infrastructure (Narasimhan, 2006; Narasimhan & Kanehiro, 1980). Constrained compressibility in the groundwater flow equation merits reconsideration and further study. Tools that are capable of modelling the three-dimensional interplay of stress, strain, and pressure, are necessary for an improved understanding of aquitard behaviour (van der Kamp, 2001).

Another common assumption in a hydrogeological analysis is that compressibility remains constant as pressure head changes. Changes in pore pressure result in changes in effective stress (total stress minus pore pressure) which control particle interaction (e.g. shear strength or volume change), with a reduction of pore pressure causing an increase in effective stress (Terzaghi, 1927). Although pore pressure is an isotropic stress tensor, effective stress is

not, and consequently under different effective stress paths the deformation and compressibility of the sample may not remain fully constrained (i.e. one-dimensional).

The compressibility of soil is also dependent upon the amount it has deformed. It is well recognized in geotechnical engineering that the compressibility of a soil is highly strain dependent with lower compressibilities at lower strain levels (Burland, 1989). Problems of strain dependency may be applicable in hydrogeologic applications. Changes in compressibility can be accounted for when using numerical techniques (Kelln et al., 2008; Rudolph & Frind, 1991). Individual soil grains are assumed incompressible, however considering their finite compressibility could be necessary for analysis in specific instances (Bishop, 1976).

2.2.1 Undrained Analysis

Geotechnical engineers routinely consider the concept of undrained analysis. This type of analysis is of greater relevance in lower permeability environments. The undrained scenario occurs when loading is applied sufficiently rapidly such that drainage of the soil does not occur during loading. Construction of civil infrastructure tends to change external stress more rapidly than would occur in natural environments (Narasimhan, 2006). The undrained analysis is therefore not routinely considered in hydrogeology, which is concerned with quantification of flow rather than instantaneous deformation. The ratio of pore pressure increments to changes in stress can be determined in a laboratory setting and are useful in the practical geotechnical applications, such as the construction of an embankment overtop clay foundations (Bishop, 1954; Skempton, 1954)

2.3 Influence of Instrumentation

The purpose of a piezometer is to determine pore pressure at a discrete point. The efficacy of an instrument's measurements depends on its compliance with the system (Gibson, 1963). Conventional Casagrande-type piezometers are insufficient for tracking rapid pore pressure changes in aquitards (Contreras et al., 2008). For a standpipe to obtain equilibrium with the surrounding formation, water must transfer between the formation and the water reservoir in the instrument. This equalization time can be impractically long in low-permeability environments.

The use of a grouted borehole annulus surrounding an installed pressure transducer has been shown as an effective way to measure rapid changes in formation pressure in low permeability formations (Vaughan, 1969). Fully-grouted boreholes also facilitates the placement of multiple vibrating-wire sensors within a single hole. After lowering sensors into position, the remaining borehole space is filled with grout, without the need for conventional sand-and-screen-intervals. Three different sources of measurement error for fully-grouted borehole include (Smerdon et al., 2014): leakage, short-circuiting; a high contrast between formation and grout properties; and evolution or degradation of grout.

Pressure measurements are representative provided the hydraulic-conductivity of the grout is not more than three-order-of-magnitude lower than the formation (Vaughan, 1969; Mikkelsen, 2002; Contreras et al., 2008). Laboratory testing of grout has also concluded that the time-lag in fully-grouted boreholes is suitable for most geotechnical applications (Simeoni, 2012). Along with determining hydraulic head, under the right geological conditions fully grouted piezometers can be used as a scale to measure changes in load at the ground surface (van der Kamp & Schmidt, 1997).

2.4 Impact of Barometric Pressure Fluctuations

The hydrogeological community has known for many decades that changes in barometric pressure have an influence on measured groundwater levels (Jacob, 1940). Continual fluctuations in atmospheric pressure propagate to the observed pore pressure records. Proper removal of barometric effects allows groundwater practitioners to better interpret flow conditions at a site (Spane, 2002). Studying the magnitude and frequency response of pore pressure to atmospheric loads allow a determination of hydrogeological properties as well as an improved understanding of the groundwater system (Butler et al., 2011).

Water is often assumed incompressible in many geotechnical and hydrogeological applications. However, for very stiff formations the soil-skeleton compressibility can be similar to that of water. The theoretical derivation of pore pressure response to atmospheric and earth tide loading has been presented by van der Kamp & Gale (1983). Pore pressure in low-permeable environments tends to be sensitive to earth tides if porosity is low. When the porosity is high, pore pressure is sensitive to atmospheric pressure (Rojstaczer & Agnew, 1989). Pore pressure

response to earth tide loading is useful for characterizing hydrogeological properties, for example, influences from fracturing (Burbey, 2010). Determination of earth tide loading efficiency is independent of the barometric response and requires an estimate of Poisson's ratio (Smith et al., 2013).

Changes in barometric pressure create a spatially distributed surface load and consequently cause a laterally constrained deformation and pore pressure response within underlying formations. The resultant change in formation pore pressure as a result of changes in barometric loading is defined by the following equation:

$$\lambda_{LE} = \frac{\Delta p}{\Delta \sigma_B} = \frac{m_v}{(m_v)+(n\beta_w)} \quad (2\text{-}3)$$

where λ_{LE} is the loading efficiency (dimensionless), and $\Delta\sigma_B$ is an incremental change in barometric pressure (kPa) and Δp is the concomitant change in formation pressure.

Different linear-regression techniques can be used to determine loading efficiency and barometric efficiency (BE = 1- λ_{LE}) (Davis & Rasmussen, 1993). The impact of loading efficiency can also be determined by a trial and error method of correcting the formation pore pressure responses for changes in barometric pressure until a smooth pore pressure record is obtained (Barr et al., 2000; Smith et al., 2013). Linear regression can determine short-term and long-term loading efficiencies. The former requires regression of pressure-increments while the latter considers the entire pressure record (Rasmussen & Crawford, 1997). These calculations are valid if the changes in water level are influenced primarily by atmospheric stresses.

Researchers have studied the theoretical response of a semi-confined aquifer to barometric loading in the frequency domain (Rojstaczer, 1988). The water level responses are low, medium, and high-frequency phenomenon. Low frequencies are a function of unsaturated zone processes while high-frequency responses are due to the confined aquifer properties. The mid-range frequency responses are due to the diffusivity of confining layers. The exact magnitude and frequency of these responses are due to material properties of the system, which can be determined analytically (Rojstaczer, 1988; Rojstaczer & Agnew, 1989). Pore pressure fluctuations can also be analyzed within the objective frequency domain method to determine both compressibility and influences from earth tide loading (Acworth et al., 2016).

2.4.1 Barometric Response Functions

The barometric response function (BRF) describes the observed transient pore pressure response in a well due to a step-change in barometric pressure. This behaviour is dependent upon hydrostratigraphy and well geometry. Theoretically, there is a unique BRF for each installation depending on the geomechanical and hydraulic properties of the formation and installation (i.e. grout). Each formation also has a typical BRF which can be used to differentiate a perfectly-confined aquifer, unconfined aquifer and wellbore storage (Spane, 2002). The BRF shape can be diagnostic for studying degree and continuity of confining layers, as well as temporal changes in vadose characteristics (Butler et al., 2011).

A VWP installed within a thick-aquitard system is anticipated to exhibit a BRF similar to a perfectly-confined aquifer with well-bore storage effects (Figure 2-1). Comparisons of linear-regression and BRF was undertaken in the Champlain Sea clays of Eastern Canada, were comparable (Marefat, et al., 2015). Correcting pore pressure results by considering the BRF and earth tide response results in a smoother pore pressure record (Rasmussen & Crawford, 1997). Proper corrections have practical implications for determining vertical gradients in low-permeability units.

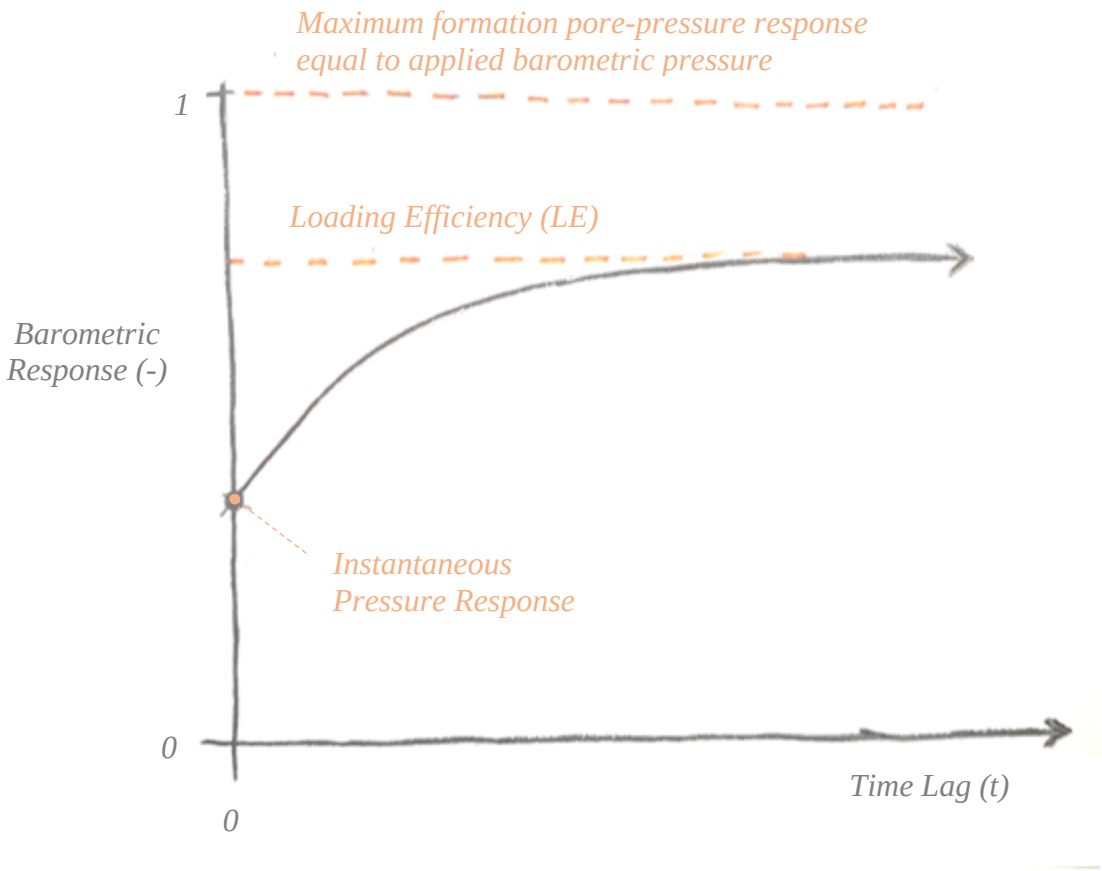

Figure 2-1 - Anticipated Barometric Response Function considering a confined aquifer with wellbore storage effects.

2.5 Previous *in situ* Aquitard Investigations

Field slug testing and laboratory permeameter testing conducted on glacial till in Saskatchewan have determined hydraulic conductivities between 1 x 10^{-11} and 1 x 10^{-8} m/s (Shaw & Hendry, 1998). Tills subject to weathering, oxidation, and fracturing tend to exhibit higher permeability (Keller, Van Der Kamp, & Cherry, 1989). Diffusion experiments *in situ* provide further evidence to constrain hydraulic conductivity (Barbour, Hendry, & Wassenaar, 2012). Natural tracers can be used to improve understanding of paleohydrogeology conditions in low-permeability environments. (Hendry et al., 2013).

The pore pressure recovery following installation, and the subsequent loading efficiency, of fully-grouted VWPs can be used to define both hydraulic conductivity and formation compressibility, respectively (Smith et al., 2016). Recent literature has suggested that both aquitard K and S_s can be determined by analyzing the transient pore pressure in fully-grouted boreholes (Smerdon et al., 2014; Smith et al., 2013). These techniques work best deep within

thick, low-permeability sequences. Both overlying and underlying aquifers complicate analysis since pressure transients are more prevalent in these formations. (van der Kamp & Maathuis, 1991).

Aquitard hydraulic conductivity can be inferred by numerical simulation of one-dimensional (horizontal) flow following borehole installation (Smerdon et al., 2014). The method is admittedly simplified yet provides a first-estimate of formation hydraulic conductivity (K_{fm}). One issue with this analysis method is a sensitivity to both formation hydraulic conductivity and compressibility of the grout. Laboratory oedometer testing is typically used to determine |compressibility. However, inaccuracies with laboratory testing will be propogated to formation K estimates. Grout must have a considerably higher permeability than the ground for the piezometer reading to have error. (Vaughan, 1969). There is, however, limited published data on the hydraulic conductivity of cement-bentonite grout mixes (Contreras et al., 2008).

3.0 METHODOLOGY

The study methodology is divided into three sections. The first section describes site conditions and existing instrumentation used to measure barometric and pore pressure data. The second section describes the heavy equipment 'point load' experimentation. The final section details the laboratory analysis used to determine grout geomechanical properties.

3.1 Barometric and Pore Pressure Data

3.1.1 Site Description

The research site is in southern Saskatchewan near the town of Weyburn. A detailed description of the site is withheld to protect client confidentiality. This location was selected since it already had instrumentation necessary to record barometric and pore pressure data. The site was initially developed for another research project focused on measuring loading efficiency and developing the hydraulic conductivity of the Pierre Shale aquitard using the time rate of recover of pore pressures following installation (Smith et al., 2013).

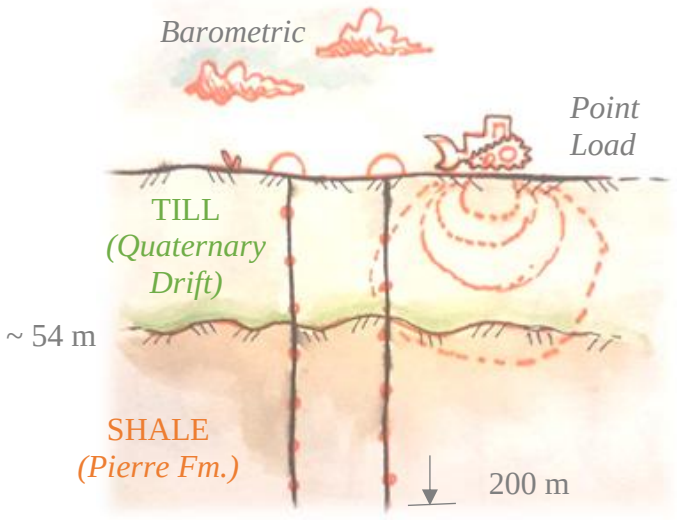

Figure 3-1 – Conceptualization of experiment (not to scale), one borehole represents the continuously cored borehole, while the other is the mud rotary borehole.

Site-specific geology was determined by both wireline geophysical logging, and core collection during drilling (SNC-Lavalin Inc., 2014). The research site lies within the Williston

Basin - a geologic structure of the more extensive Western Canadian Sedimentary Basin. The site stratigraphy consists of quaternary deposits overlying shale bedrock (Figure 3-1).

The quaternary layers are till deposits characterized as the Saskatoon group and Sutherland groups. Both groups are comprised of a lower and upper proglacial basal till with overlying non-glacial sediment. The various till groups and formations are differentiated based upon carbonate content, Atterberg limits, stratigraphic position of the till, bounded weathered zones or non-glacial sediments. (Christiansen, 1992). The first-encountered surficial geology is identified as the Saskatoon group. The top 8.7 m was described as silty till which exhibited iron-straining, overlying predominantly clay and silt. Two silt seams were identified within the Saskatoon Group. The Sutherland Group, also primarily silt and clay, was identified at 44.7 m below ground surface.

Drilling encountered bedrock deposits at 53.8 m below ground surface. They are Late-Cretaceous aged Pierre Shale; described as dark grey, unoxidized, and very hard. Core samples showed evidence of shell fragments and bioturbation. The Cretaceous shales are approximately 500 m thick with thin layers of interstitial sandstone and siltstone (Carr, 2010). Underlying the unconformity beneath the Cretaceous shales is Devonian limestones and dolostones. This study focuses on the upper most 200 m of the formation where instrumentation was installed. Underlying aquifers can influence pore pressure response (Anochikwa et al., 2012), although due to the depth and the hydraulic conductivity of the shale at this location they are unlikely to be a factor in this study.

Two fully-grouted boreholes were installed to a depth of 200 m in July 2014 (SNC-Lavalin Inc., 2014). The first borehole was undertaken using continuously coring (CC) drilling methods. Mud rotary (MR) techniques were used to drill the second borehole. A string of ten vibrating-wire piezometers (VWP) were placed within the borehole annulus which was subsequently grouted over the full depth of the borehole. The VWPs were affixed to a 51 mm (2-inch) steel tremie line to ensure placement at the predetermined depth (Figure 3-2). The VWPs were selected to have an increased pressure range at greater depths. This increased range capability also results in a loss of resolution (Table 3-1). Grout was placed with a tremie pipe to fill remaining void space within the hole.

Polyurethane cables connected each VWP to a data logger at the ground surface. The data logger used to record piezometer measurements was a GeoKon LC-2x16 (Model 8002-16-1) with 3,555 arrays of storage capacity. Depending on the selected recording frequency the data logger could be filled in approximately one day (30-second recording intervals) or up to two-and-a-half months (30-minute recording intervals). The data logger at the top of each borehole was covered by a fibreglass dome and a metal frame to protect from heavy equipment operating in the area.

Barometric pressure was measured and recorded with a Solinst Barologger Gold which had a nominal resolution of 1 mm H_2O. The barologger was suspended about 1m above ground surface within a fibreglass shelter. The extent to which the sensor was protected from temperature fluctuations is unknown, which may have an impact on the barometric readings. Visual inspection of recorded barometric pressure and temperature indicates that temperature influences are negligible.

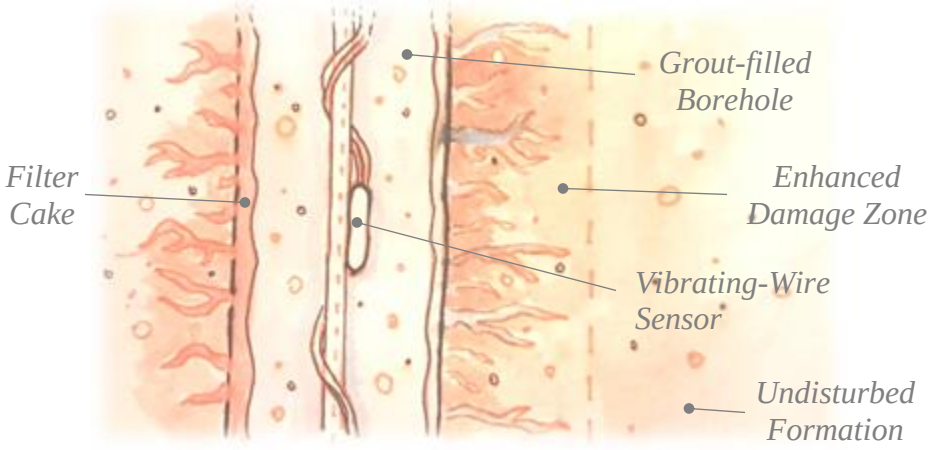

Figure 3-2 – Conceptualization of a fully-grouted borehole piezometer with focus on single sensor (not to scale).

Table 3-1 – Installed vibrating-wire sensor specifications.

VWP Installation Depth (mbgs)	VWP Sensor Model	Nominal Resolution (mm H_2O)
10 & 20	GeoKon 4500S – 300 kPa	8.9
30 & 40	GeoKon 4500S – 700 kPa	17.8
50 & 60	GeoKon 4500S – 1 MPa	25.5
70, 80, 90, 100, 110, & 120	GeoKon 4500S – 2 MPa	51.0
130, 140, 150, 160, 170, & 180	GeoKon 4500S – 3 MPa	76.5
190 & 200	GeoKon 4500S – 4 MPa	127.4

3.2 Localized Surface Loading Experiments

Vehicular loads were used to generate an instantaneous surface load which would also generate a pore pressure response in the shallower VWPs. This approach is similar to that used by Jacob (1939) who analyzed pore pressure changes near a rail line to determine formation properties. A similar approach was used by van der Kamp and Schmidt (1997) who used a loaded gravel truck to serve as a point load near a piezometer in a thick clay formation. The instrument set-up to record both barometric, and pore pressure during localized surface loading is identical to the preceding subsection (Section 3.1.1). Two loading experiments were conducted, nearly a year apart, using two separate pieces of heavy equipment.

The initial localized surface loading experiment occurred on October 7th, 2015. This preliminary test intended to determine the capabilities of instrumentation at the site. Before the initial experiment, it was not known if the surface load was sufficient to create a measurable pressure response within the VWPs. The load was a triaxial water truck, with an estimated weight of 100,000 lbs (45,360 kg). A measuring tape was used to determine the length (18.3 m) and width (2.4 m) of the water truck. During the experiment the weather was overcast. Precipitation in the days leading up to the experiment resulted in muddy field conditions. The load was placed in 11 different positions for approximately 15 minutes each (Figure 3-3).

A second localized surface loading test occurred on August 4th, 2016. The rationale for running a second test was to utilize a larger and more concentrated load. The intent was to induce more substantial stress at greater depth, relative to the first test. The duration of the applied load was also increased to allow more time for the VWPs to reach equilibrium with the surrounding formation. The maximum measurement frequency (i.e. 30 seconds) was used. The second experiment also had more accurately measured geometry than the first. There had been very little precipitation in the days leading up to the second loading test.

The point load considered for the second loading experiment was a D8T Caterpillar Bulldozer. According to equipment specification sheets, the D8T weighs approximately 86,900 lbs (39,420 kg). The tracks of the D8T are 3.2 m long and 0.6 m wide (Caterpillar, 2017). Placement of the load was in four positions surrounding the piezometer nest (Figure 3-4). It remained in each location for no less than an hour. Between loading intervals, the D8T was removed from the site to allow pressure to dissipate back to static conditions.

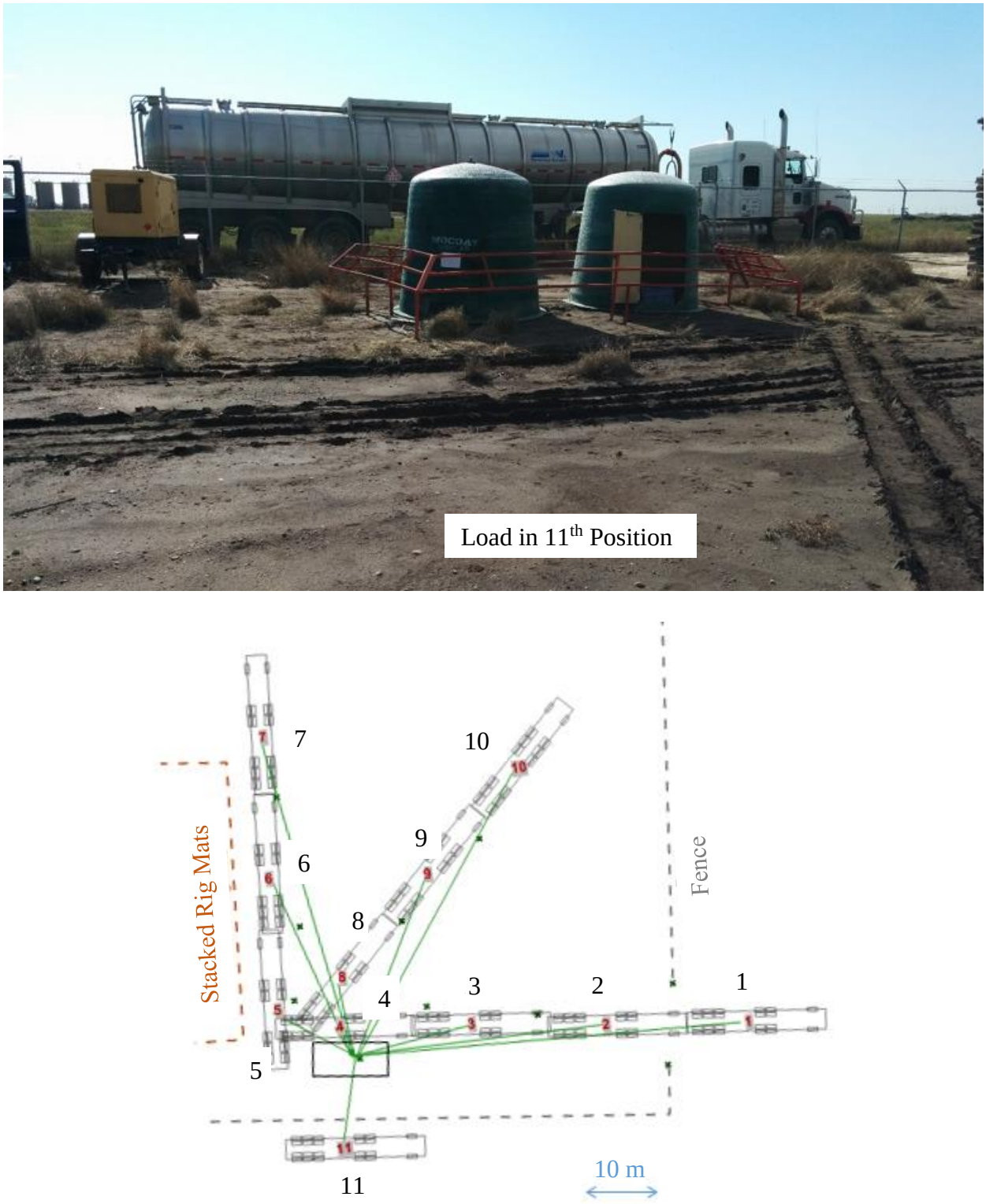

Figure 3-3 - Water truck surface load experiment showing 11 loading positions.

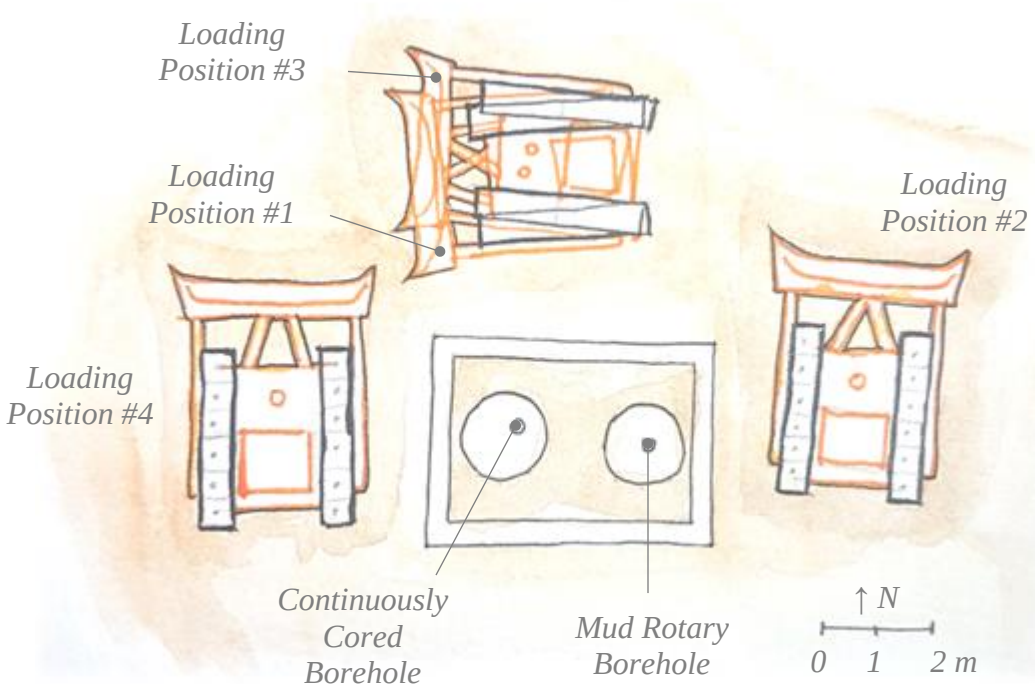

Figure 3-4 - D8T surface loading experiment.

3.3 Grout Properties

The estimation of formation hydraulic conductivity obtained from analyzing the response of grouted VWPs following installation is sensitive to the assumed compressibility of the grout (Smerdon et al., 2014). Conventional laboratory testing tends to overestimate compressibility. Oedometer testing subjects a sample to greater strain than *in situ* deformations due to barometric loading (Clayton, 2011). The grout testing program outlined below attempts to measure grout compressibility at relatively low levels of strain.

A grout mixture was made by manually stirring cement and bentonite into water in a plastic container. The grout was mixed with a ratio of 96% cement and 4% bentonite, which is the ratio used in the field when installing the VWP instrumentation. The bentonite used was Cetco Super Gel-X Extra High Yield Drilling Fluid. The cement used was Lafarge Type HS Kalicrete which is a high sulphate resistant Portland cement, and was provided by the drilling contractor who installed the site instrumentation. Additional amounts of bentonite and cement were measured with a scale and added to the mixture to achieve the desired specific gravity of 1.7.

The grout mixture was poured into two separate PVC tubes approximately 330 mm long and 35 mm in diameter. The grout was placed in approximately 50 mm high lifts and mechanically disturbed to minimize entrapped air. The grout was left to cure in a temperature and humidity controlled room for more than 24 days. There is a difference between curing conditions in the laboratory and the subsurface, most notably, grout cured *in situ* would be completely saturated. After curing, a handsaw was used to cut the grout into smaller sections. The edges of each sample were smoothed and levelled with a metal file. Dimensions of the grout samples are included in Table 3-2.

Table 3-2 – Dimensions of grout samples used for acoustic testing.

Sample #	Mass (g)	Dia. (mm)	Length (mm)	Density (kg/m^3)
2.3	174.86	35	103	1764.5
2.2	181.69	35	103	1833.4
2.1	216.79	35	132	1707.0

The elastic properties of the grout were measured using an acoustic pulse as per ASTMD2845-08. (ASTM, 2005). The standard is a method using ultrasonic pulses to estimate

static rock properties. Axial stress, which can be manually adjusted, is applied and a transmitter sends an acoustic wave, originating from one side of the sample (Figure 3-5). A receiver on the other side detects the wave after it passes through the rock. A digital oscilloscope processes the signal to determine the travel velocities of both compressional and shear waves.

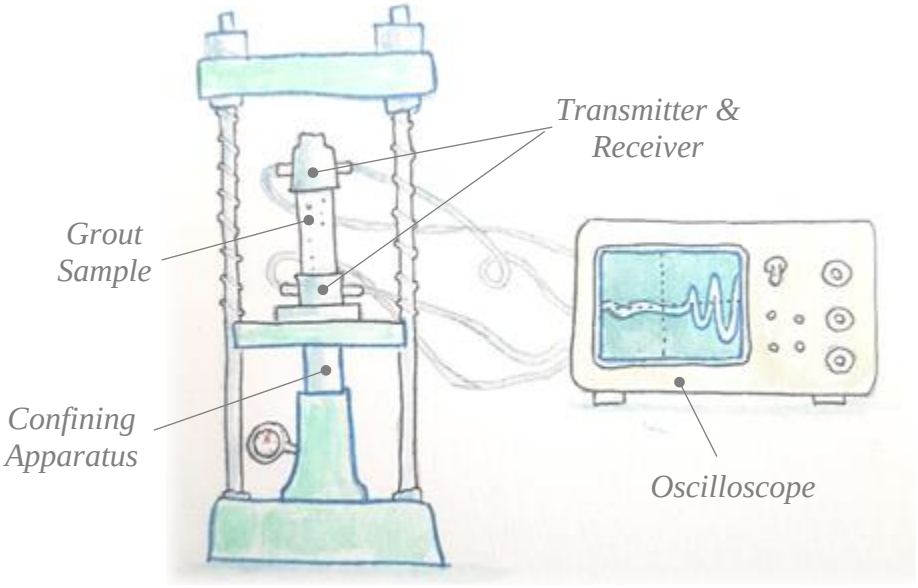

Figure 3-5 – Schematic of laboratory set-up to determine acoustic wave velocities through grout samples.

4.0 RESULTS

The three data sets which were in the analyses for this study include the VWP barometric and pore pressure time data during barometric loading, VWP pore pressure response to the localized surface loading and the measurement of the properties of the grout. These data sets are presented and discussed in this chapter. Detailed records associated with each of these measurements are included in digital form with the thesis.

4.1 Barometric and Pore Pressure Data

The record of barometric pressures measured since the installation of the VWPs is presented in Figure 4-1. Barometric pressure fluctuates continuously exhibiting apparent seasonal trends. Table 4-1 presents a summary of typical ranges of changes in barometric pressure that have been observed based on a range of different recording intervals used by the data logger.

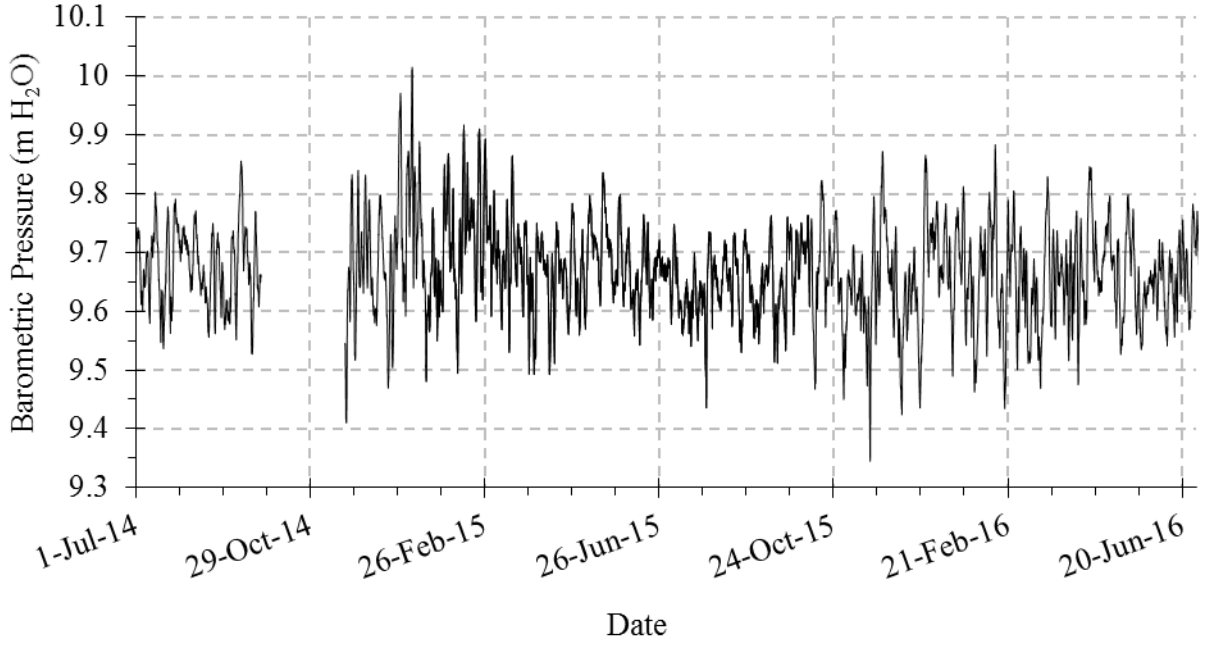

Figure 4-1 – Measured barometric pressure record.

Table 4-1 – Changes in barometric pressure for six different barometric recording intervals.

Recording Interval (minutes)	Duration (days)	Minimum Barometric Increment (mm H_2O)	Maximum Barometric Increment (mm H_2O)	Mean Barometric Increment (mm H_2O)
5	7.8	-9.0	9.6	-0.033
5	55.7	-7.3	9.1	-0.002
10	6.0	-11.0	12.0	0.052
30	263.9	-32.5	35.5	0.008
30	349.8	-26.2	43.0	0.003
30	551.8	-32.5	35.5	0.006

***Note** – the different recording intervals represent data sets that are complete, without missing data records.

The records of VWP pressure recovery following installation are presented in Figure 4-2 for both instrumented boreholes. The relatively rapid recovery of the shallow VWPs located within the glacial till is notable. VWPs installed within shale recovered more rapidly in the continuously cored borehole (approximately 3 months) relative to the mud rotary hole (over a year).

Figure 4-3 illustrates the response of the VWP measurements to barometric pressure fluctuations for VWPs at varying depths in both boreholes. There is a different transient response between the cored and mud rotary boreholes. There are gaps in the data set due to data logger issues. There may be problems with the recorded data near data gap intervals due to a weakened battery. One limitation of the data is the decreasing resolution of the VWPs with depth (Table 3-1). Below a depth of 60m, the resolution of VWP instrumentation is larger than anticipated changes in barometric pressure. Clearly, the response to barometric pressure is more evident in the shallow boreholes while in deep boreholes the barometric response is evident yet masked by noise.

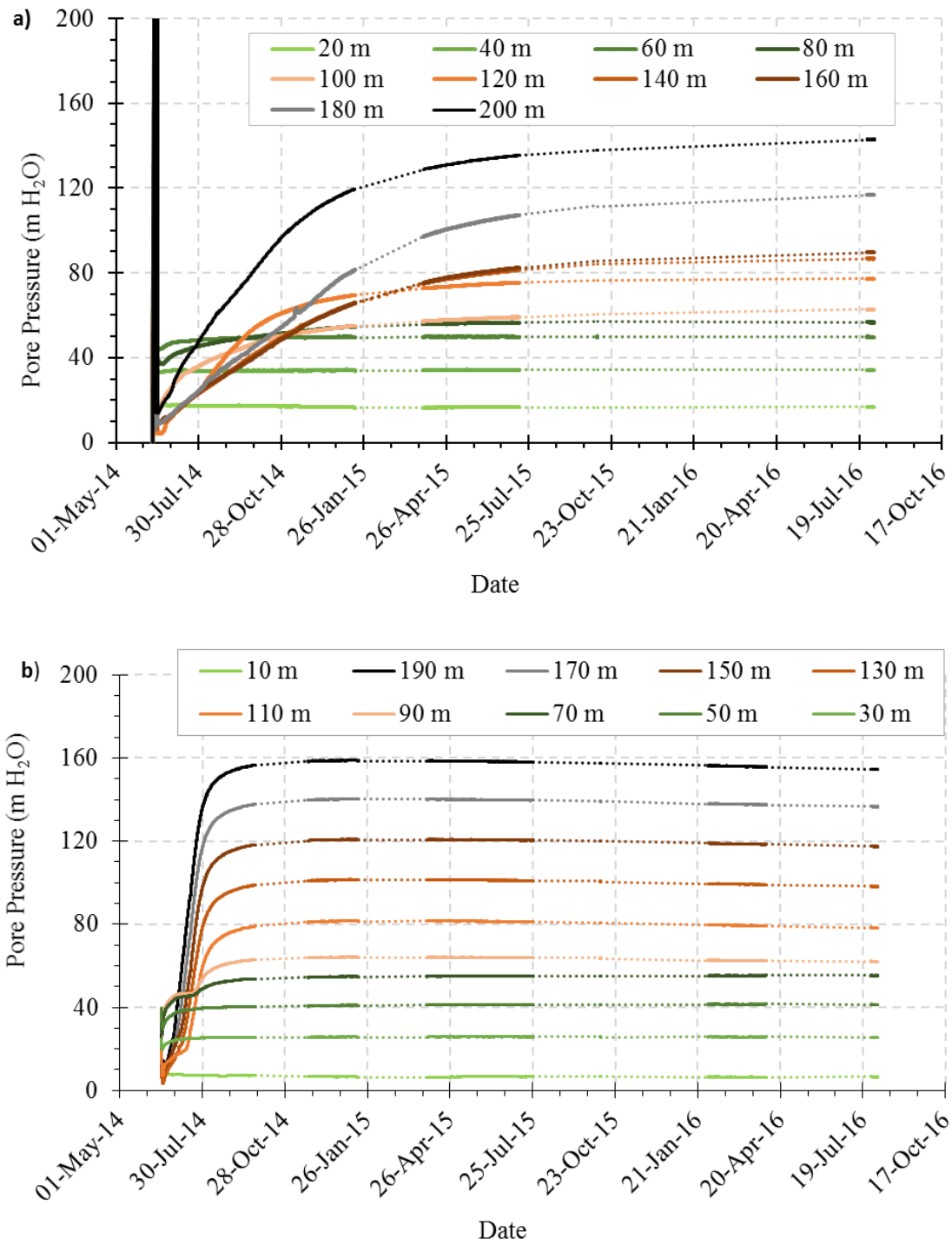

Figure 4-2 – VWP pore pressure records since installation for the a) mud rotary borehole (top), and b) continuously cored borehole (bottom). Dotted lines indicate data gaps. The till-shale interface is at 54 m.

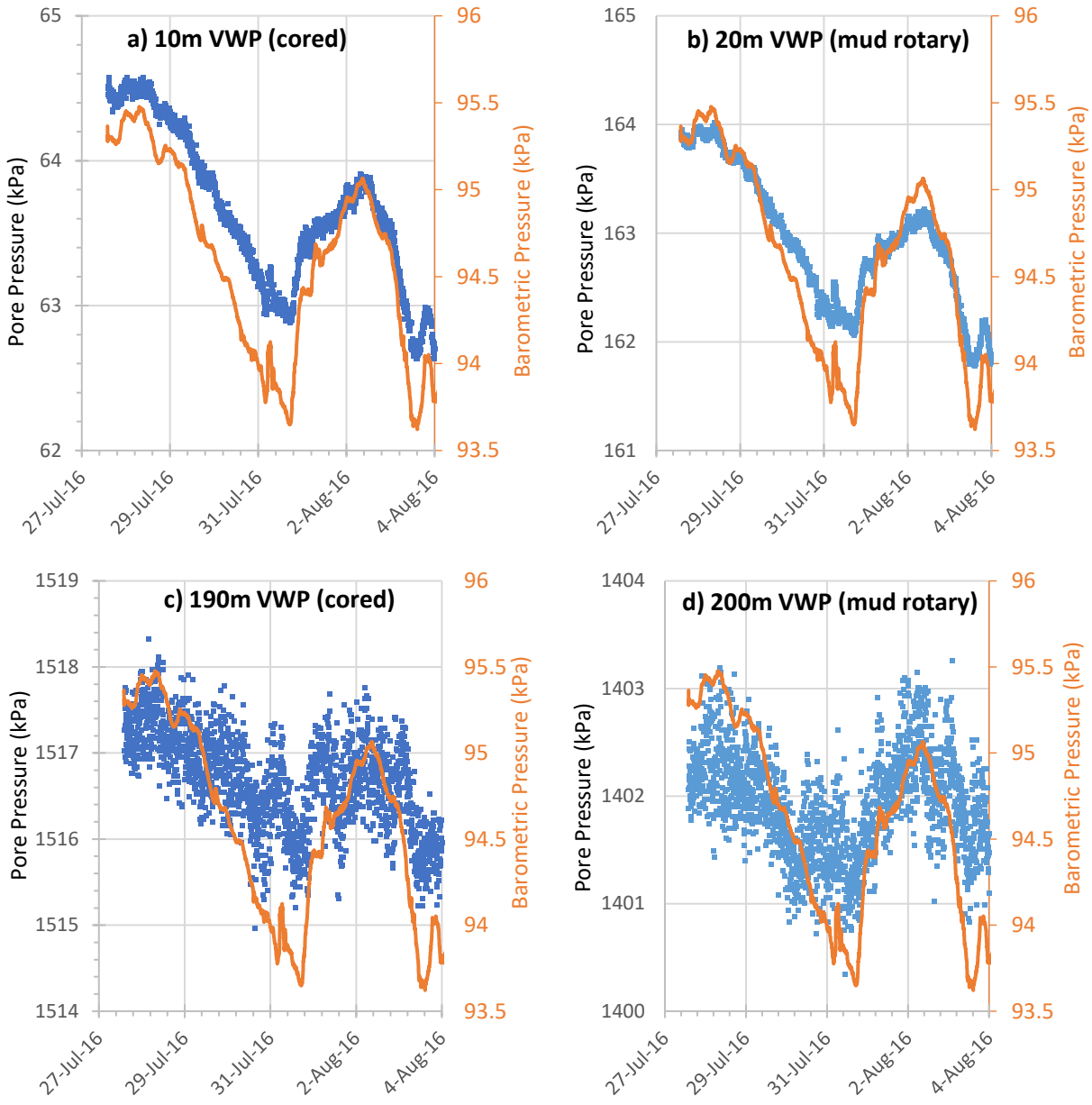

Figure 4-3 – Abridged pressure records showing response to barometric pressure and instrument resolution for the 10m (top left), 20m (top right), 190m (bottom left) and 200m (bottom right) VWPs.

4.2 Localized Surface Loading Experiment Results

The purpose of the initial surface loading test was to evaluate whether the VWPs would respond to this type of loading. The observed responses as shown in Figure 4-4 show a clear response of the shallow VWPs to the surface load. The data loggers were set to record at a higher frequency just prior to the arrival of the water truck at the site with recording intervals adjusted from 30 minutes to 1 minute. This did not allow for a clear record of formation pressures prior to loading and consequently the static pore pressures response were not well defined. Furthermore, the exact location of the point load was estimated with a handheld GPS device and are not sufficiently accurate for superposition of the Boussinesq solution. The distribution of the truck load between the front, middle and rear axles was also unknown. The load remained in each loading position for approximately 15 minutes. Based on the observations made for loading intervals 4 and 8 it appears that the formation pressures were still increasing at this time. The first test highlighted limitations associated with the loading tests and allowed improvements to be made in the protocol for the second test. Only data from the second test were used for analsysis.

The barometric pressure during the second surface-loading test was reasonably consistent over the duration of the experiment; with a mean pressure of 9.666 m and standard deviation of 0.006. Distances between the heavy equipment and protective casing around the VWP nest were measured with a tape measure; the geometry of the second loading test was improved from the initial test. There does appear to be some measurement drift in the 20m VWP, which is not apparent in the other boreholes (Figure 4-5). Temperature variations could cause instrumentation drift during point loading experiments (van der Kamp & Schmidt, 1997), although since only one sensor was affected it is more likely related to the geology. Although the D8T had a lower ground contact pressure, the areas of contact are more concentrated. A pore pressure response to the surface loading was observable to a depth of 40 m. It is difficult to discern impacts from the loading beyond this depth for two reasons. Firstly, the ‘stress bulb’ magnitude response decreases with depth. Secondly, instrumentation at greater depth needs to measure higher pressure, and there is a corresponding loss of resolution.

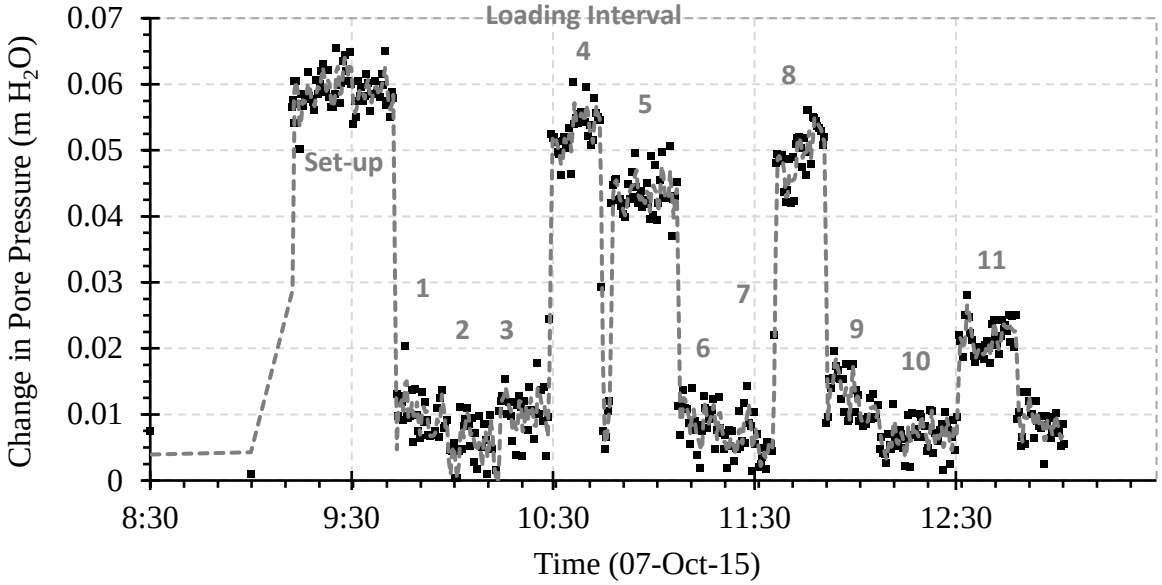

Figure 4-4 – First Point Loading Experiment pressure data from the 10 m VWP in the core borehole during each of the eleven 15-minute loading intervals. (dashed line is a two-point moving average).

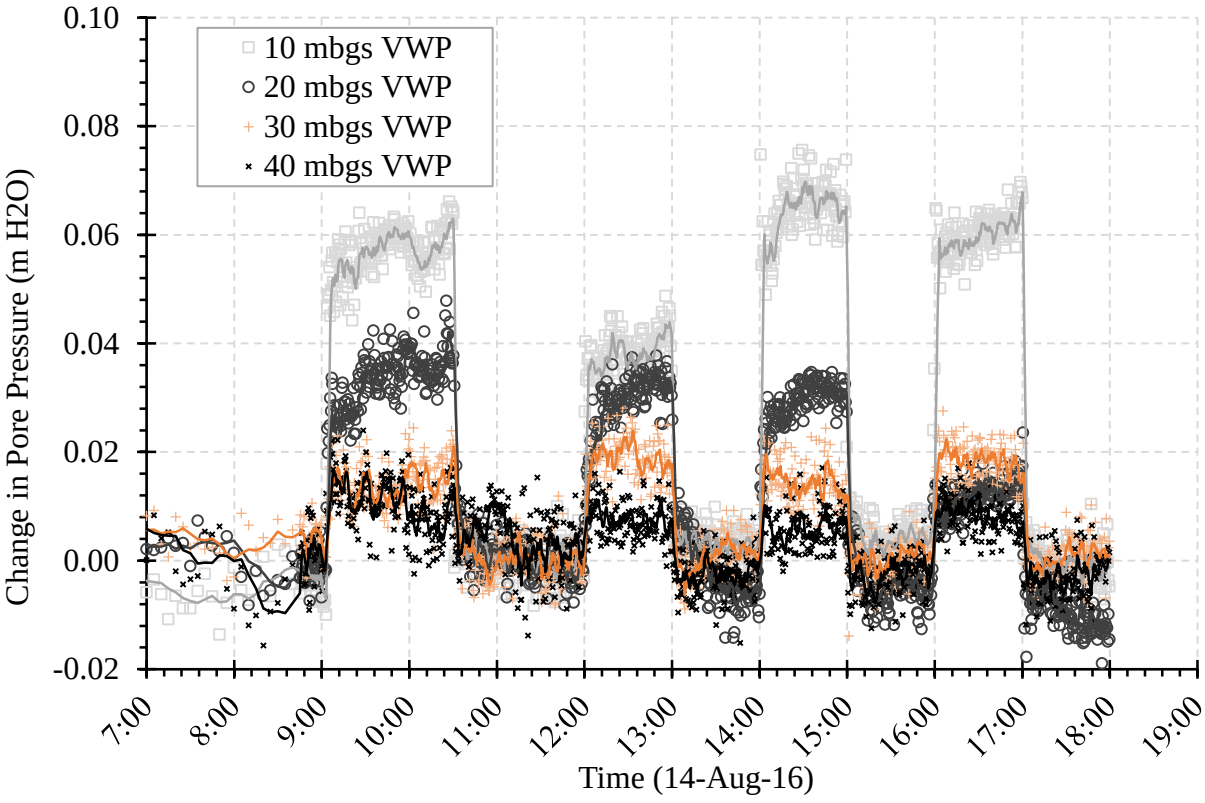

Figure 4-5 – Second Point Loading Experiment (solid lines indicate a 6-period moving average for slightly easier visualization of loading influence).

4.3 Grout Properties

One-dimensional consolidation testing of the borehole grout samples was conducted previously in 2011. The full set of laboratory data from this testing is presented in Appendix A. The laboratory testing conducted as part of this research used an oscilloscope to determine the time elapsed for compressional (P-wave) and shear (S-wave) waves to pass through the grout sample from the transmitter to a receiver. Travel time offsets due to the geometry of transmitter and receiver locations, are 7.84 μs and 12.26 μs for the P-wave and S-wave, respectively. These offsets are a constant correction subtracted from the measured acoustic wave travel times. The dynamic elastic moduli of the samples can then be calculated by (ASTM, 2005):

$$V_p = \frac{L_p}{T_p} \tag{4-1}$$

$$V_s = \frac{L_s}{T_s} \tag{4-2}$$

$$E_d = \frac{\rho V_s^2 (3V_p^2 - 4V_s^2)}{(V_p^2 - V_s^2)} \tag{4-3}$$

$$v_d = \frac{(V_p^2 - 2V_s^2)}{2(V_p^2 - V_s^2)} \tag{4-4}$$

where V_p (m/s) is the P-wave travel velocity, V_s (m/s) is the S-wave travel velocity, E_d is the dynamic Young's modulus (kPa), ν_d (dimensionless) is the dynamic Poisson's ratio.

In order to compare the elastic modulus to the constrained compressibility used often in this study the following relationship between constrained compressibility and elastic modulus was used:

$$m_v = \frac{(1+v)(1-2v)}{E(1-v)} \tag{4-5}$$

where ν is the Poisson's ratio (dimensionless), E is Young's modulus (kPa), and m_v is the constrained compressibility (kPa^{-1}). Grout geomechanical properties are summarized in Table 4-2.

Table 4-2 – Geomechanical grout properties calculated from acoustic laboratory testing.

Sample #	Confining Axial Load (tons)	P-wave Travel Time (µs)	S-wave Travel Time (µs)	Dynamic Young's Modulus, E_d (kPa)	Dynamic Poisson's Ratio, ν_d (-)	Dynamic Constrained Compressibility $m_{v\text{-}d}$ (kPa^{-1})
2.3	1.00	37.4	65.8	1.7×10^7	0.2804	8.3×10^{-8}
2.3*	1.00	38.6	68.7	1.5×10^7	0.2884	9.0×10^{-8}
2.2	0.50	37.6	66.5	1.7×10^7	0.2843	8.1×10^{-8}
2.2	0.75	37.6	66.5	1.7×10^7	0.2843	8.1×10^{-8}
2.2*	1.00	37.5	66.6	1.7×10^7	0.2875	8.1×10^{-8}

**sample broke when confining stress was applied*

There did not appear to be a change in the elastic properties of the material over the range of loads applied during these tests. Both of the samples developed a crack that effectively broke the sample in half when the axial load was equal to or greater than 1 ton (or 740 kPa for a 35 mm diameter sample). Even with the crack, consistent acoustic travel-times were measured.

There is limited information in the literature on the compressibility for cement-bentonite grout mixtures used for borehole backfill. Smith et al. (2013) reported a grout compressibility of 4.8×10^{-5} kPa^{-1} from oedometer testing; however, the authors acknowledge that the testing was done at a lower confining stress that would be experienced *in situ*. Furthermore, oedometer testing subjects the grout to larger strains than *in situ*. For this reason, compressibility in other studies vary by an order-of-magnitude to assess the sensitivity of numerical models to grout properties (Smerdon et al., 2014). The range of grout constrained compressibility from acoustic testing (8×10^{-8} kPa^{-1}) is lower than that observed for the till (1×10^{-6} kPa^{-1}) and in the same order of magnitude as reported values of compressibility for the shales (3×10^{-7} kPa^{-1}) as determined from barometric loading efficiency (Hendry Geosciences Inc., 2014).

5.0 ANALYSIS AND DISCUSSION

5.1 Stress Relationship between Barometric and Pore Pressures

This section outlines the conceptual framework used to explain the observed pore pressure response to atmospheric pressure fluctuations. Changes in barometric pressure ($\Delta\sigma_B$, kPa) are distributed over a large area, which effectively constrains deformations to the vertical direction within the formation (Figure 5-1). As a result, one-dimensional compressibility of the formation ($m_{v\cdot fm}$, kPa^{-1}) can be inferred from barometric loading efficiency (λ_{LE}, Equation 5-1) as described by Equation 5-1:

$$m_{v\cdot fm} = \frac{\lambda_{LE}\cdot n_{fm}\cdot \beta_w}{1-\lambda_{LE}} \quad (5\text{-}1)$$

where βw (kPa^{-1}) is the bulk compressibility of water and n_{fm} (dimensionless) is the porosity of the formation.

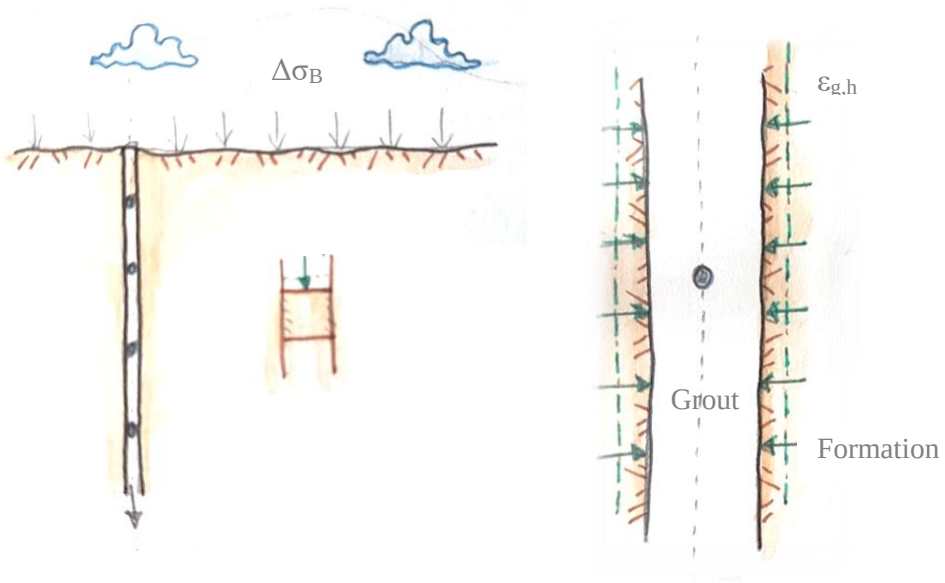

Figure 5-1 - Conceptual model of loading efficiency vertical strain (left) and borehole horizontal strain (right).

Two different methods for estimating the loading efficiency are compared in this paper: a visual inspection method, and the interpretation of barometric response functions (BRF). The visual inspection methods assumes that the pore pressure response measured by the VWPs is

always in equilibrium with the formation pore pressure (i.e. no time lag). In reality, however, the vertical barometric load also results in a change in lateral stress which must be transmitted into the grouted annulus. This stress transfer causes an initial instantaneous pore pressure response. Since this initial pore pressure response is not in equilibrium with the formation pore pressure there is also a time dependent recovery of the observed pressure. This time delayed pore pressure response will be characterized using the BRF method described below. The magnitude of the horizontal strain, and subsequent pore pressure response, within the grouted annulus will be a function of the stiffness and Poisson's ratio contrast between the formation and the bentonite grout within the borehole. The significance of the horizontal deformation in the grout will be discussed following the BRF analysis.

5.1.1 Visual Inspection Method to Determine Loading Efficiency

One published technique of determining loading efficiency is through visual inspection (Smith et al., 2013). In this method, the loading efficiency is determined by adjusting λ_{LE} within a plot of the corrected pressure (p*) until the smoothest variation of corrected pore pressure (as judged visually) is obtained (Figure 5-2). The corrected pressure is calculated as follows:

$$p^* = [p_t - B_{avg}] - \lambda_{LE}[B_t - B_{avg}] \quad (5\text{-}2)$$

where p* is the corrected pore pressure (kPa), p_t is the detrended and uncorrected pore pressure record (kPa), B_{avg} (kPa) is the average the average barometric pressure for the data set, and B_t (kPa) is the detrended barometric record. Once λ_{LE} is known, the formation compressibility can be determined by Equation 5-1.

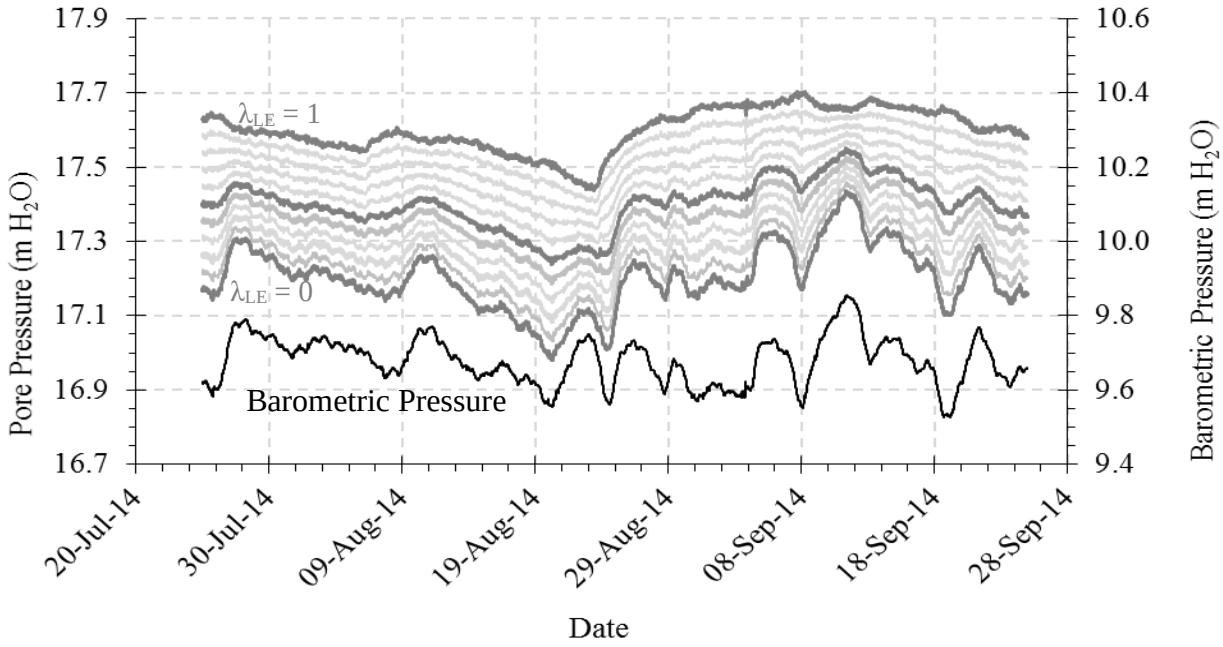

Figure 5-2 - Visual inspection method for 20 m VWP within the mud rotary borehole. Grey lines illustrate 0.1 increments of λ_{LE} used in Equation 5-1. A λ_{LE} value of 0.8 results in the smoothest line and is thus the inferred loading efficiency.

The visual inspection method, as well as other linear approaches mentioned in the literature review, assume that the pore pressures measured in the VWP are in instantaneous equilibrium with the formation pressures without any time lag between the formation and grouted borehole. This issue is less prevalent if the objective is only to determine loading efficiency. However, if the goal is to smooth pore pressure records, then corrections should consider the barometric response function.

5.1.2 Barometric Response Functions

The barometric loading function quantifies the transient relationship between pore pressure and barometric fluctuations. A deconvolution technique (Rasmussen & Crawford, 1997) can be used to determine BRFs, assuming atmospheric pressure is the only external stress which causes pore pressure fluctuations. After linear trends in the data are removed - a process referred to as 'detrending'- the measured changes in pore pressure and barometric pressure are used to populate a set of linear equations as shown in Equation 5-3 below:

$$\begin{bmatrix} W_m^* \\ W_{m+1}^* \\ W_{m+2}^* \\ \vdots \\ W_n^* \end{bmatrix} = \begin{bmatrix} \Delta B_1 & \Delta B_2 & \Delta B_3 & \cdots & \Delta B_m \\ \Delta B_2 & \Delta B_3 & \Delta B_4 & \cdots & \Delta B_{m+1} \\ \Delta B_3 & \Delta B_4 & \Delta B_5 & \cdots & \Delta B_{m+2} \\ \vdots & \vdots & \vdots & \ddots & \vdots \\ \Delta B_{n-m+1} & \Delta B_{n-m+2} & \Delta B_{n-m+3} & \cdots & \Delta B_n \end{bmatrix} \begin{bmatrix} \alpha_1 \\ \alpha_2 \\ \alpha_3 \\ \vdots \\ \alpha_m \end{bmatrix} \quad (5\text{-}3)$$

where the single matrix W^*_m to W^*_n is the detrended pore pressure record (kPa), ΔB is the change in barometric pressure (kPa), n represents the total number of readings in a data set, and m represents the maximum time-lag. A multiple-linear-regression method is then used to determine a single matrix (α_1 to α_m, unitless). The variation of the cumulative α_i values ($\Sigma\alpha_i$) with time represents the barometric response function (BRF). The ideal BRF would result in a plateau in $\Sigma\alpha_i$ value equal to λ_{LE}. However, since some interpretation of the BRF is required this function is described more generally as follows:

$$A(i) = \sum_{j=1}^{i} \alpha(j) \quad (5\text{-}4)$$

Data records of both pore pressure and barometric pressure are available for the intervals provided in Table 5-1. It is recommended that the BRF be developed using a minimum of two weeks of pore pressure data, collected at an ideal time step of less than one hour (Toll & Rasmussen, 2007). BRFs were developed for each data set using the multiple-linear regression approach, however not all BRFs were considered representative of the formation and grouted system.

Table 5-1 - Intervals of collected barometric and pore pressure data for BRF deconvolution.

Data Set	Start Date	Duration (days)	Recording Frequency (mins)
1	25-Jul-14	62	30
2	24-Nov-14	53	30
3	31-Mar-15	49	30
4	16-May-15	71	30
5*	1-Feb-16	63	30
6	27-Jul-16	7.7	5

Note: *For reference, drilling of boreholes occurred between June 11 and 16, 2014.*
**due to some recording error, only corehole data was recorded during data set 5*

BRF deconvolution using the multiple linear regression method requires a data set of adequate duration, with a linear trend. The first data set is inappropriate because the recording interval occurred soon after borehole installation. The trend of this data set was therefore similar

to a Theis recovery type curve and consequently is not amenable to BRF deconvolution. The sixth dataset was inadequate because the data set contains only one week of recordings collected at 5-minute intervals. The change in barometric pressure over five minutes is relatively small compared to the precision of the measurement instrumentation (Table 3-1) A representative BRF with greater resolution may have worked for a 5 minute recording interval if the data had been collected for a longer duration.

BRF results from the remaining four datasets are relatively consistent and are visually similar to BRFs typical of a theoretical confined aquifer with well-bore storage (Spane, 2002). At greater depths (> 60 m), the instrument resolution decreases and calculated BRFs are dominated by numerical noise (Figure 5-3). For this reason, the BRF interpretation undertaken in subsequent analysis will use average values of the initial instantaneous response to loading (α_1) as well as loading efficiency (λ_{LE}) from the second, third, fourth, and fifth dataset. Given the noise in deeper VWP's the loading efficiency was taken as the average barometric response from the time lag 10 to 15 hours. Multiple-linear regression results for all six datasets are included in Appendix B.

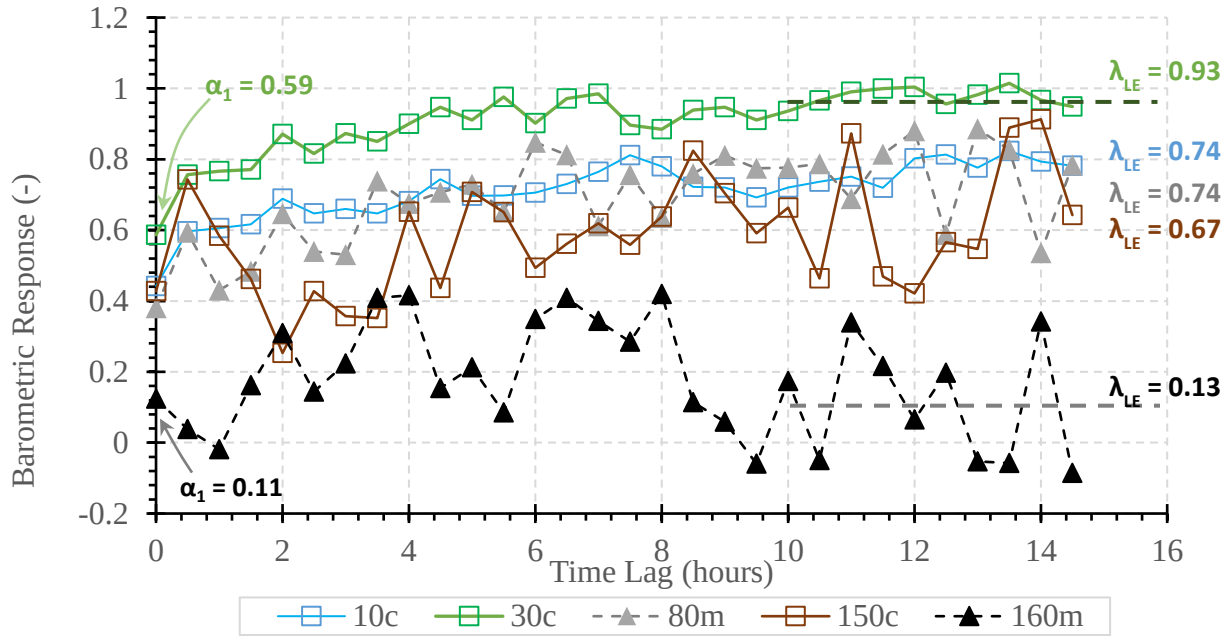

Figure 5-3 - Representative barometric response functions at varying depths, c and m qualifiers represent the corehole and mud rotary hole, respectively.

It is useful to visualize a depth profile of the BRF characteristics, α_1 and λ_{LE} (Figure 5-4). The visual-inspection loading efficiencies determined by Hendry Geosciences Inc. (2014) are included for comparison. The loading efficiencies from visual inspection could not be obtained below a depth of 90 m in the mud rotary borehole. It is hypothesized that a compressible layer develops along the borehole annulus in the mud rotary boreholes and beyond 90 m this creates difficulties in the assumption of instantaneous equilibrium between formation and the monitored pore pressure. Such a compressible layer could be attributed to either mud filter-cake build-up (Moench & Hsieh, 1985), or stress-related damage to the borehole. This anomalous behavior was not observed in the continuously cored borehole.

Instrument sensitivity and time-weighted-averaging were essential considerations in this analysis, although the body of this report does not present exhaustive results (Appendix B). Using a time-weighted-average helps remove noise from pore pressure trends. However, if averaging is applied before deconvolution, the BRF characteristics are skewed. These inaccuracies are especially when identifying the instantaneous pressure response (α_1).

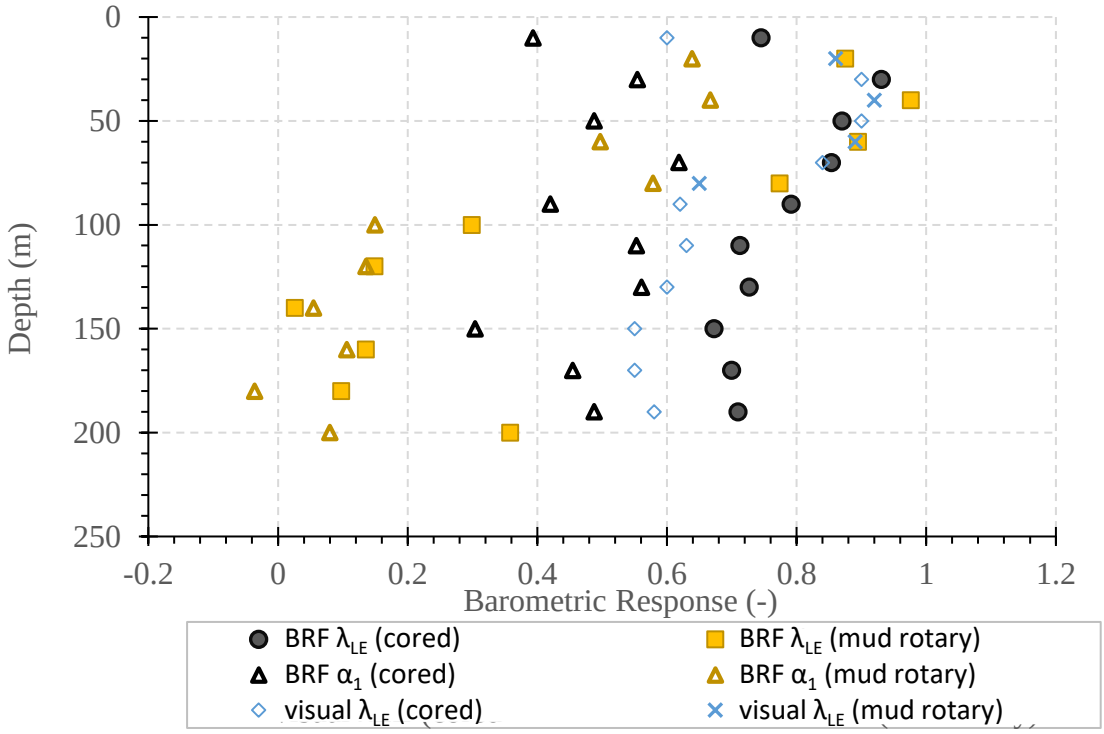

Figure 5-4 - Depth profile of BRF characteristics compared to visual method from determining LE. (Circles represent data from the continuously cored hole while triangles represent the mud rotary borehole).

Modelling Loading Efficiency (λ_{LE})

Numerical modelling was undertaken to demonstrate that the loading efficiency could be replicated within a finite element model. Naylor (1974) presents a method which allows excess pore pressures to be explicitly calculated from computed volumetric strains in a total stress analysis. For a stiff soil, the pore fluid exhibits a finite compressibility, meaning the pore fluid will undergo volumetric compression when the soil is subject to an applied load. Since part of the load is supported by the soil skeleton, the change in pore water pressure is not equal to the applied total mean stress. Naylor (1974) demonstrated through strain compatibility that the total stress (undrained) moduli can be equated from drained moduli with the following equations:

$$\frac{E_u}{E'} = \frac{3(1-2v')+E'/K_a}{2(1-2v')(1+v')+E'/K_a} \tag{5-5}$$

$$v_u = \frac{(1-2v')(1+v')+\frac{E'v'}{K_a}}{2(1-2v')(1+v')+\frac{E'}{K_a}} \tag{5-6}$$

where E_u is the undrained Young's Modulus (kPa), E' is the drained Young's Modulus (kPa), v_u is the undrained Poisson's ratio (dimensionless), and v' is the drained Poisson's ratio (dimensionless). K_a is the apparent stiffness of the pore fluid (kPa), which is a function of the stiffness of soil grains (K_{grains}, kPa) and compressibility of pore fluid (β_w, kPa^{-1}):

$$K_a = \frac{1}{n\beta_w+\frac{(1-n)}{K_{grains}}} \tag{5-7}$$

A finite element load-deformation analysis can be undertaken using the undrained moduli (E_u, and v_u) as input parameters to calculate the volumetric strain ($\varepsilon_\forall$, unitless). The change in pore pressure (Δp, kPa) can then be calculated from volumetric strain by:

$$\Delta p = K_a \varepsilon_\forall \tag{5-8}$$

For the case of barometric loading, m_v' can be derived from loading efficiency (Equation 5-1). The constrained compressibility can be related to an effective Young's modulus by assuming an effective Poisson's ratio. Total stress moduli can then be determined through Equations 5-6 and 5-7. An effective Poisson's ratio of 0.3 was selected to calculate total stress

moduli, which is in the range of Poisson's ratio for both shale and granular soils (Gercek, 2007). The depth profile of loading efficiency and corresponding total stress moduli for the site are summarized in Table 5-2.

Table 5-2 – Relationship between effective moduli and total stress moduli (v' = 0.3).

Depth	λ_{LE}	porosity	m_v'	E'	K_a	E_u	v_u
10	0.74	0.35	4.70×10^{-7}	1.58×10^{6}	6.21×10^{6}	1.78×10^{6}	0.4607
20	0.88	0.36	1.16×10^{-6}	6.40×10^{5}	6.04×10^{6}	7.30×10^{5}	0.4815
30	0.93	0.37	2.28×10^{-6}	3.25×10^{5}	5.88×10^{6}	3.73×10^{5}	0.4899
40	0.98	0.36	6.76×10^{-6}	1.09×10^{5}	6.04×10^{6}	1.27×10^{5}	0.4966
50	0.87	0.34	1.05×10^{-6}	7.10×10^{5}	6.39×10^{6}	8.09×10^{5}	0.4807
60	0.89	0.33	1.29×10^{-6}	5.76×10^{5}	6.59×10^{6}	6.59×10^{5}	0.4845
70	0.85	0.32	8.60×10^{-7}	8.64×10^{5}	6.79×10^{6}	9.83×10^{5}	0.4782
80	0.77	0.33	5.19×10^{-7}	1.43×10^{6}	6.59×10^{6}	1.61×10^{6}	0.4654
90	0.79	0.33	5.76×10^{-7}	1.29×10^{6}	6.59×10^{6}	1.46×10^{6}	0.4683
110	0.71	0.33	3.76×10^{-7}	1.97×10^{6}	6.59×10^{6}	2.21×10^{6}	0.4553
130	0.73	0.33	4.04×10^{-7}	1.84×10^{6}	6.59×10^{6}	2.06×10^{6}	0.4577
150	0.67	0.36	3.40×10^{-7}	2.18×10^{6}	6.04×10^{6}	2.43×10^{6}	0.4484
170	0.70	0.31	3.33×10^{-7}	2.23×10^{6}	7.01×10^{6}	2.50×10^{6}	0.4531
190	0.71	0.29	3.26×10^{-7}	2.28×10^{6}	7.50×10^{6}	2.55×10^{6}	0.4547

A simple model was formulated in SIGMA\W to verify that Naylor's methodology adequately captures the change in pore pressure defined by loading efficiency (Figure 5-5). E_u and v_u from Table 5-2 were used as input parameters for the total stress load-deformation analysis, although the model only considered the three shallowest VWPs.

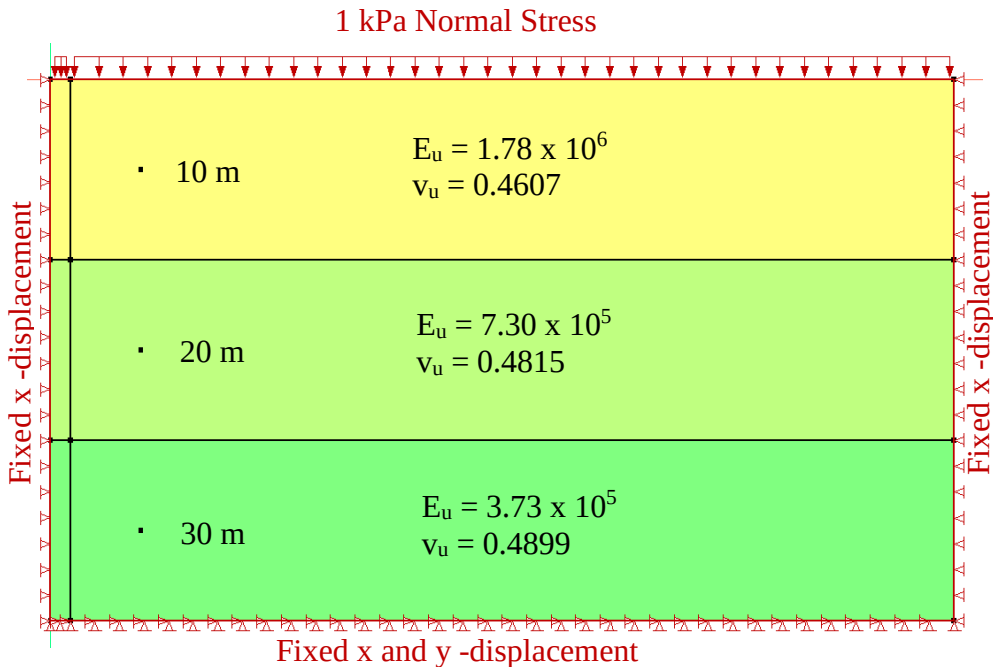

Figure 5-5 – Loading efficiency verification model set-up.

Volumetric strains were computed and multiplied by K_a to determine the change in pore pressure (Table 5-3). It was found that the calculated change in pore pressure was equivalent to the defined loading efficiency. In the following section this modelling methodology will be expanded upon to consider the presence of a grouted borehole.

Table 5-3 – Loading efficiency verification model results.

Depth (m)	Volumetric Strain, ε_v	Pore Pressure = $\varepsilon_v * K_a$ (kPa)
10	1.20E-07	0.74
20	1.45E-07	0.88
30	1.58E-07	0.93

Modelling the Instantaneous Pressure Response (α_1)

Following the naming convention of Rasmussen & Crawford (1997), α_1 describes the instantaneously observed pressure response in a fully-grouted borehole due to a step change in barometric pressure. The α_1 is interpreted to be due to differences in compressibility between the grouted annulus and the surrounding formation. A modelling exercise was undertaken to back-analyze the α_1 response in order to estimate the *in situ* grout compressibility.

A Sigma/W model was set-up to determine instantaneous pressure response (Figure 5-6). The geometry is axisymmetric which extends 100 metres in the x-direction (radial) and 200 metres in the y-direction (depth). The model set a one-metre finite element size throughout, although, with further refinement specified near the borehole. The element width in the grouted section is 0.0795 m, which corresponds with the borehole radius. Although the grouted section was only one element wide, the sensitivity of this modelling assumption was tested and determined to not have an impact on the resulting volumetric strains. The finite element mesh used for analysis had 21105 nodes and 20800 elements. Boundary conditions constrained the model from deforming laterally on the left (axisymmetric centre) and right (far-field) edges. The bottom edge of the model was constrained in both lateral and vertical directions, thereby not allowing displacements. A 1 kPa stress was applied normal to the top surface, to mimic a step change in barometric pressure.

The model was divided into 14 layers and input parameters were assigned to each layer based upon the total stress moduli specified in Table 5-2. Volumetric strains along the borehole axis were computed by the load-deformation model and converted to pore pressure using Naylor's methodology.

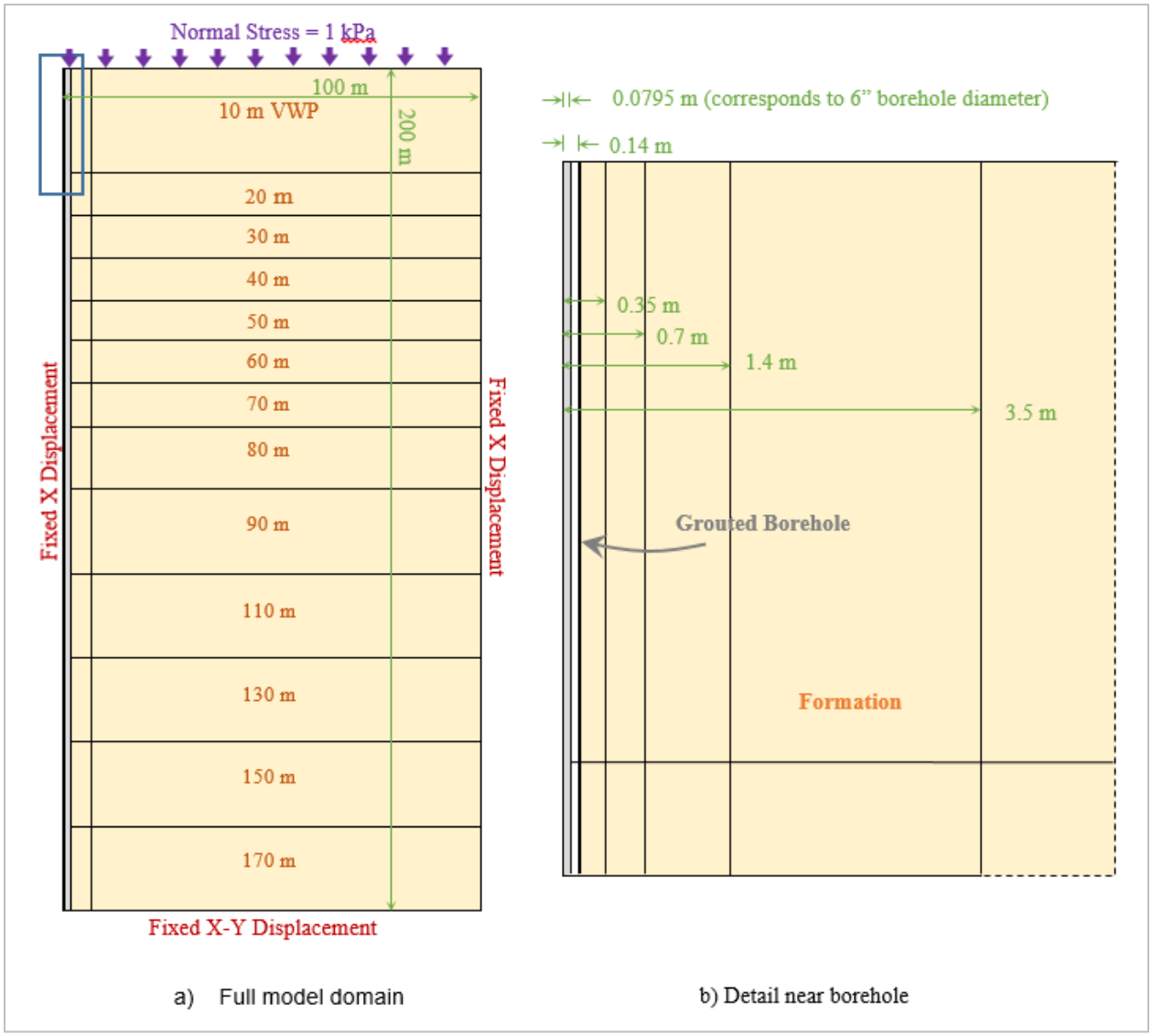

Figure 5-6 – Instantaneous pressure response model set-up.

The total stress moduli (both E_u and ν_u) within the grouted region was varied to match simulated pore pressures with the observed α_1 depth profile (Figure 5-7). The total stress moduli were then converted back to drained moduli using Naylor's equations (equation 5-5 and 5-6). This back-analysis for α_1 suggests that the one-dimensional drained compressibility of grout is approximately 2×10^{-7} kPa^{-1} (Table 5-4). This estimate is consistent with the acoustic grout testing (Table 4-2), and less compressible than oedometer testing (4.8×10^{-5} kPa^{-1}, Smith et al., 2013).

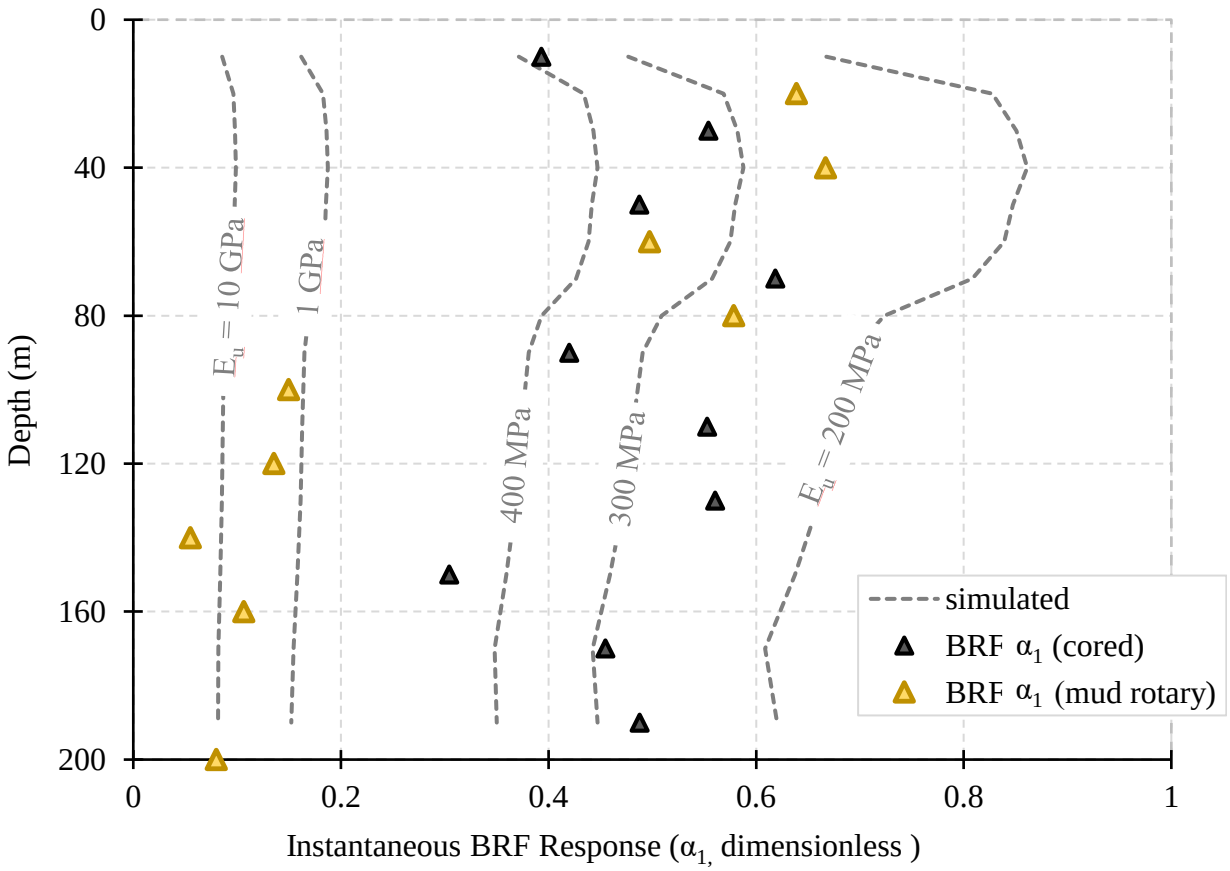

Figure 5-7 – Simulated instantaneous pressure response within the grouted borehole (ν_u = 0.495).

Table 5-4 – Summary of grout moduli estimates from BRF instantaneous pressure (α_1) simulations.

ν_u (-)	E_u (kPa)	$m_{v\text{-}u}$ (kPa^{-1})	ν' (-)	E' (kPa)	m_v' (kPa^{-1})
0.300	3 x10^{7}	2.5 x10^{-8}	0.248	2.89 x10^{7}	2.9 x10^{-8}
0.450	3 x10^{6}	8.8 x10^{-8}	0.382	2.86 x10^{6}	1.8 x10^{-7}
0.490	6 x10^{5}	9.7 x10^{-8}	0.470	5.85 x10^{5}	2.8 x10^{-7}
0.495	3 x10^{5}	9.9 x10^{-8}	0.490	2.99 x10^{5}	2.0 x10^{-7}

5.2 Transient BRF Analysis

Since there is differing strain within the grouted borehole and the surrounding formation, there is also a pore pressure difference. This hydraulic gradient between the formation and grouted annulus will result in water flow between the two. Transient flow will continue until equilibrium conditions are met. Atmospheric pressure is constantly changing, which means the borehole-formation water transfer is continuously occurring. It is however possible to replicate the transient flow characterized by the BRF. Initial pressure conditions within the borehole are dictated by α_1, and flow occurs until the borehole reaches the formation pressure, $\lambda_{LE.}$ Another scenario where flow occurs between formation and borehole is immediately following the borehole installation (Smerdon et al., 2014). Both these transient scenarios can be analyzed to inversely determine hydraulic properties of the borehole-formation system.

Four simplified flow models were set-up similar to that described by Smerdon et al. (2014). The modelling process considered VWP response at four distinct depths, and two values for grout compressibility (Table 5-5). Each model is axisymmetric around the centreline of the borehole. The SEEP/W models were 50 metres radially (x-direction) and one-metre thick (y-direction). Transient simulations considered both the pressure recovery after borehole installation as well as the barometric response function.

Grout and Formation hydraulic conductivity were set as the same value. Previous modelling of pressure recovery surrounding a grouted-in VWP found that the transient response is most sensitive to grout compressibility and formation hydraulic conductivity (Smerdon et al., 2014). Throughout this modelling process these sensitivities were reaffirmed. Grout hydraulic conductivity only influenced the simulated transients when it was three-orders-of-magnitude different from the formation hydraulic conductivity which is consistent with literature findings (Contreras et al., 2008). Including a compressible filter cake in simulations did alter the transient results however this analysis is beyond the scope of this project and is not discussed in detail.

Table 5-5 - Hydraulic conductivity inferred from simulations of transient pressure response.

VWP Depth (m)	Borehole	Compressible Grout (m_{v-g} = 4.8 x 10^{-5} kPa^{-1})		Stiff Grout (m_{v-g} = 1.0 x 10^{-7} kPa^{-1})	
		K_{fm} determined from BRF transient (m/s)	K_{fm} determined from Installation-Recovery (m/s)	K_{fm} determined from BRF transient (m/s)	K_{fm} determined from Installation-Recovery (m/s)
20	Mud rotary	1 x 10^{-9}	1 x 10^{-10}	1 x 10^{-11}	1 x 10^{-12}
30	Cored	1 x 10^{-9}	1 x 10^{-11}	1 x 10^{-11}	1 x 10^{-13}
80	Mud rotary	1 x 10^{-9}	1 x 10^{-12}	1 x 10^{-12}	1 x 10^{-14}
150	Cored	1 x 10^{-10}	1 x 10^{-12}	1 x 10^{-12}	1 x 10^{-14}

In all cases, the best fit to the observations required a higher formation hydraulic conductivity (K_{fm}) to match the transient BRF response than that required to match the pressure recovery-following-installation (Figure 5-8). The K_{fm} determined by replicating the BRF response is at least one order-of-magnitude more hydraulically conductive compared to the installation-recovery model. This infers that the near-borehole hydraulic conductivity is different from the undisturbed formation. Such a difference could be due to stress-related borehole damage, a mud filter-cake, or the grout hydraulic conductivity. Regardless, the simulating the BRF transient response may not yield representative value of $K_{fm,}$ but could glean additional insight into the influences a borehole may have on observed pressure response.

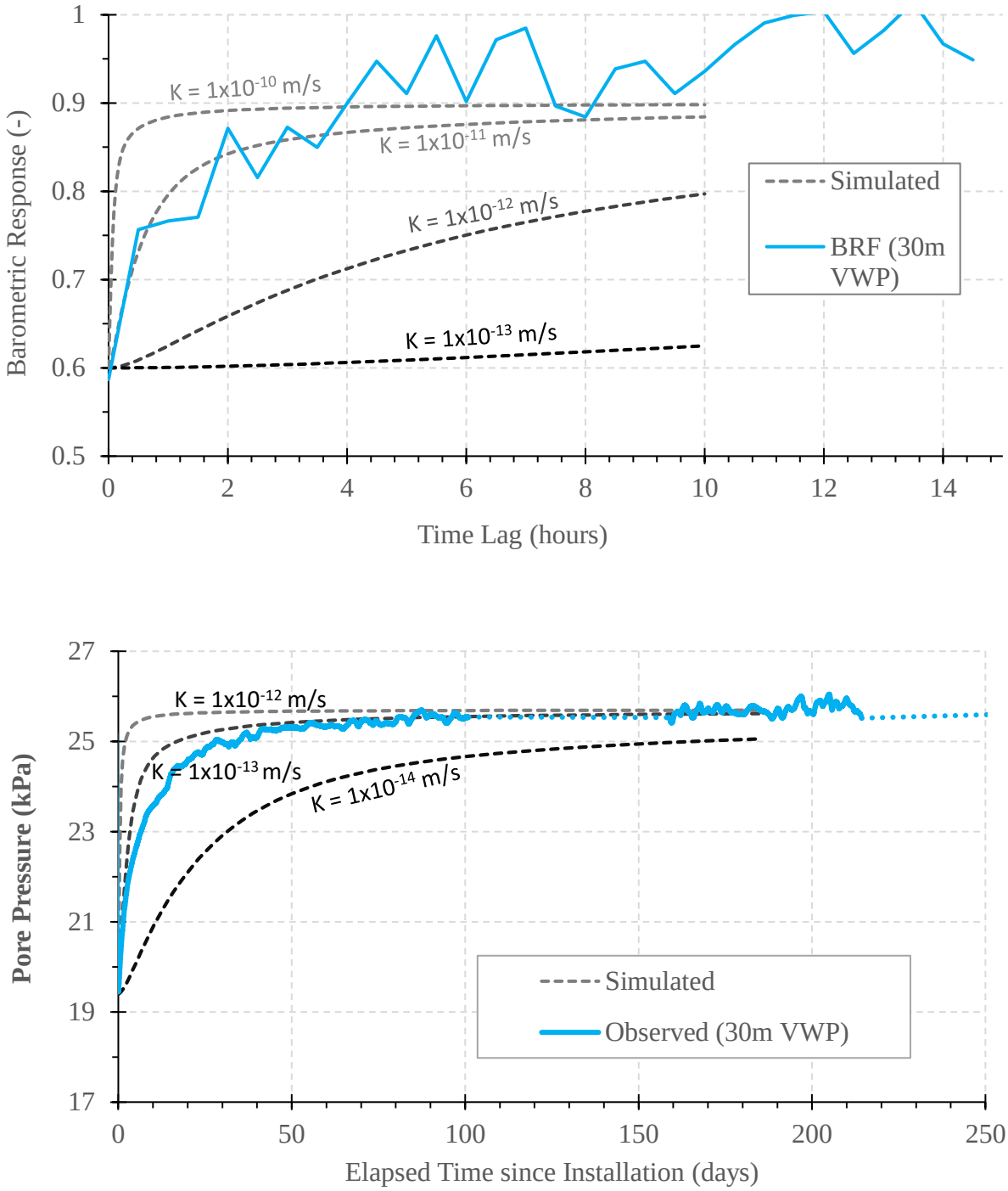

Figure 5-8 – Transient modelling results for the 30m VWP considering $m_{v\text{-}g} = 1x10^{-7}$ kPa^{-1} for the BRF (top) and recovery-following-installation (bottom).

5.3 Localized Surface Loading Experiment Analysis

Conceptually, a change in stress due to a vehicle load will be instantaneously supported by the soil and pore fluid. Loading by heavy equipment can be considered a discrete point compared to the extensive lateral application of atmospheric pressure. The distribution of stress can be estimated by a derivation of the Boussinesq solution (van der Kamp & Schmidt, 1997), or some similar techniques. The stress distribution will cause a differential change in pore water pressure, which will induce flow to occur within the formation both vertically and horizontally. In addition to this redistribution of induced pore pressure within the formation there is also the instantaneous response and following time lag within the VWP (Figure 5-9). These two transient responses are re-initiated during unloading as there is an instantaneous incremental change in pore pressure within the formation as a result of unloading and gradual re-equilibration of the formation pressures back to the pre-loading distribution as well as the instantaneous and transient pore pressure change within the grouted borehole.

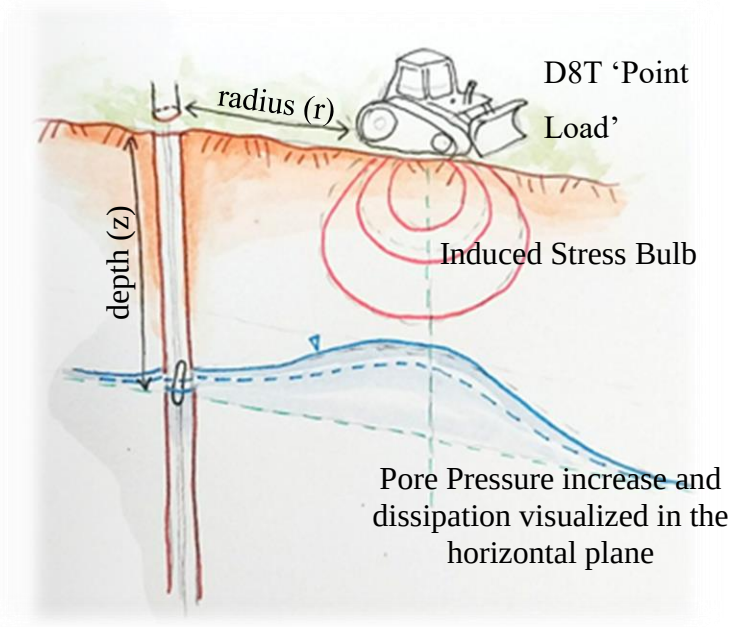

Figure 5-9 –Conceptual model of induced pressure response due to heavy equipment loading.

5.3.1 Predicting the Magnitude of Induced Stress

The stresses induced beneath the heavy equipment were estimated using both analytical solutions as well as numerical simulations. The loading experiment conducted on August 4th, 2016 consisted of four loading-unloading periods. The first loading positions was left in place for 1.5 hours and then removed for the same duration. The rest of the loading and unloading intervals were one-hour in duration. The distance from the borehole to the centroid of the surface load is summarized in Table 5-6. Pore pressure changes due to surficial loading were only observed within shallow (<50 m deep) VWPs. The contact between till and shale was interpreted to occur at a depth of 54 m; it is therefore not possible to differentiate a pressure response between the till and shale VWPs.

Table 5-6 – Summary of point load experiment geometry.

Loading Interval	Loading Duration (hours)	Average distance to Mud Rotary Borehole (m)	Average distance to Cored Borehole (m)
Load 1	1.5	5.67	5.12
Load 2	1	4.10	6.60
Load 3	1	5.88	5.39
Load 4	1	7.03	4.45

The Boussinesq solution for a point load on an isotropic half space was used to estimate stresses beneath a piece of heavy equipment. The stress influence and subsequent pore pressure response diminish with depth and radial distance away from the point load (Boussinesq Solution summarized by Kirkby & Pickett, 2006):

$$\Delta\sigma_z = \frac{3Mz^3}{L^5 2\pi} \tag{5-9}$$

$$\Delta\sigma_x = \frac{M}{2\pi}\left\{\frac{3x^2z}{L^5} - (1-2\nu_u)\left[\frac{x^2-y^2}{Lr^2(L+z)} + \frac{y^2z}{L^3r^2}\right]\right\} \tag{5-10}$$

$$\Delta\sigma_y = \frac{M}{2\pi}\left\{\frac{3y^2z}{L^5} - (1-2\nu_u)\left[\frac{y^2-x^2}{Lr^2(L+z)} + \frac{x^2z}{L^3r^2}\right]\right\} \tag{5-11}$$

where z is the assessment depth (m), M is the mass of the point load (kg), x and y represent the Cartesian distance from the point load (m), v_u is the undrained Poisson's ratio

(dimensionless), r and L are functions of x, y and z (m). A derivation of the Boussinesq equation is used to determine the mean change in confining stress which is then converted to a pore pressure change (van der Kamp & Schmidt, 1997). The combination of Equations 5-9, 5-10, 5-11, and 2-3, reduce to:

$$\Delta p = \frac{\lambda_{LE}\, M\, z(1+v_u)}{3\pi\,(r^2+z^2)^{\frac{3}{2}}} \tag{5-12}$$

To determine the distribution of pore pressures induced by loading (p_{load}, kPa) it is more apt to multiply the mean total stress bulb (σ_T, kPa) by Skempton's (1954) pore pressure parameter B (B, dimensionless):

$$p_{load} = B * \sigma_T \tag{5.13}$$

The relationship between Skempton's B and loading efficiency (λ_{LE}) is summarized by:

$$B = \frac{3\lambda_{LE}}{1+2(\frac{v_u}{1-v_u})} \tag{5.14}$$

Depending on the undrained Poisson's ratio of the formation, the value of Skempton's B, may be larger than the loading efficiency (Table 5-7). For calculations of pore pressure distribution, it was assumed that the undrained Poissons ratio slightly less than 0.5 therefore Skempton's B and loading efficiency are of similar magnitude. Figure 5-10 illustrates that for a range of effective Poisson's ratio, provided the Young's modulus is low enough, the undrained Poisson's ratio is close to 0.5 and can be assumed so.

Table 5-7 – Relationship between loading efficiency and Skempton's B parameter.

Depth	λ_{LE}	B (v_u = 0.4)	B (v_u = 0.45)	B (v_u = 0.495)
10	0.74	0.96	0.85	0.75
20	0.88	1.13	1.00	0.89
30	0.93	1.20	1.06	0.94
40	0.98	1.25	1.11	0.99

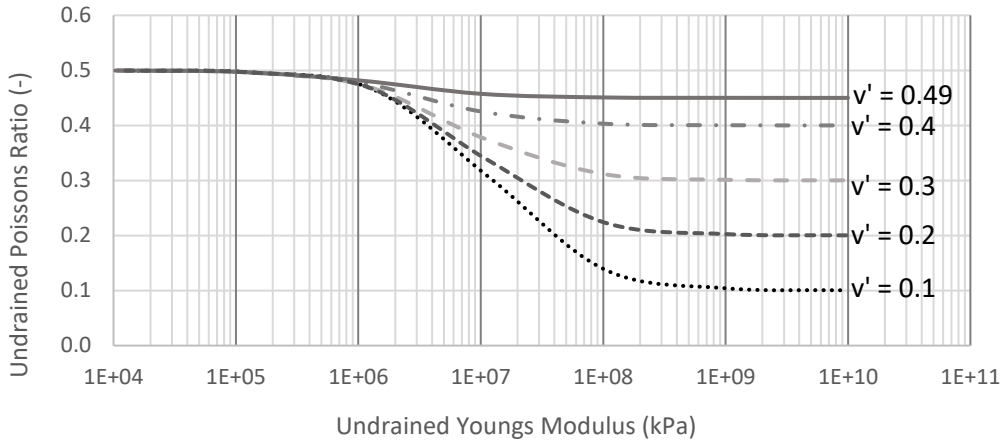

Figure 5-10 – Relationship between effective Poisson's ratio and undrained moduli.

Difficulties were encountered attempting to match the Boussineq solution to the loading test pressure data (Figure 5-10). Although it was possible to achieve a match with the 10m. The deeper data was underestimated. For this reason, the stress bulb beneath the heavy equipment was modeled using SIGMA/W, which allowed the load to be considered distributed over an area. Reference to the localized surface load as a point load is misleading since heavy equipment loads are spread over the areas where tires, or track, are in contact with the ground (Smith & Dickson, 1990). The effective contact area and ground pressure for a D8T are 3.91 m² and 89.6 kPa, respectively (Caterpillar, 2017).

In addition to considering a distributed load, modelling the mean total stress bulb in SIGMA/W also allowed for simulating anisotropic ground conditions. During the modelling process, it was found that the magnitudes of elastic moduli were inconsequential, but the ratios between moduli had an influence on the simulated stress bulb. Equations which define the relationships between anisotropic moduli are presented below (Clayton, 2011):

$$\nu_{hh}^{u} = 1 - \frac{E_h^u}{2E_v^u} \tag{5-15}$$

$$\nu_{vh}^{u} = 0.5 \tag{5-16}$$

$$G_h = \frac{E_h^u}{2(1+\nu_{hh}^{u})} \tag{5-17}$$

where ν_{hh}^{u} (unitless) is the Poisson's ratio of horizontal strain imposed by horizontal strain in the normal direction, ν_{vh}^{u} (unitless) is Poisson's ratio related to horizontal strain imposed by vertical strain, E_h^u (kPa) is undrained Young's modulus for loading in the horizontal direction, E_v^u (kPa) is undrained Young's modulus for loading in the vertical direction, and G_h(kPa) is shear modulus for distortion in the horizontal direction. Other anisotropic moduli exist, but only five are required to fully-characterize the elastic stress-strain behavior.

A comparison between pressure data observed during the loading experiment, and calculated stress bulbs is presented in Figure 5-11. The BRF data presented earlier (Figure 5-3) suggests that it takes approximately 6 hours for the borehole to equalize with the surrounding formation. It is therefore expected that pore pressures observed during the 1 to 1.5 hour loading tests do not reach the full equalization. The calculated stress within the formation (Δp_f, kPa) induced by surface point loading can be summarized by:

$$\Delta p_f = \frac{\alpha_p}{\alpha_1} \tag{5-18}$$

Where α_p (kPa) is the instantaneous pressure rise from point loading, and α_1 is the instantaneous pressure rise from BRF analysis. The inferred mean-total-stress from loading is included in Figure 5-11. The best fit with calculated stress bulbs occurs when considering distributed load over a transversely isotropic material, with a E_h^u/E_v^u ratio somewhere between 2 and 2.5. Further analysis will consider a mean stress bulb with the anisotropic ratio (E_h^u/E_v^u) of 2 (Figure 5-12).

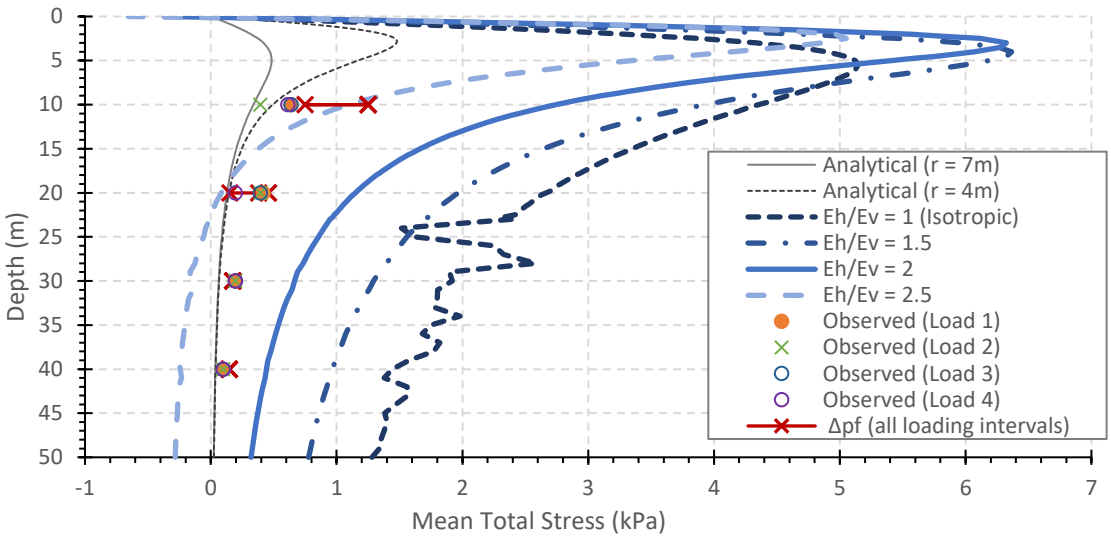

Figure 5-11 – Comparing localized surface load observed pore pressure response with mean total stress determined from analytical and numerical solutions.

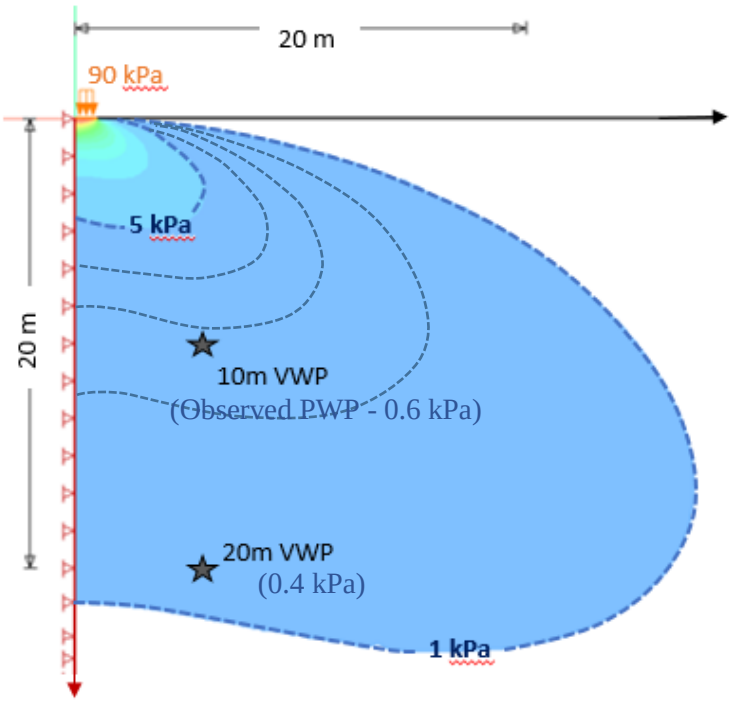

Figure 5-12 – Simulated mean total stress bulb using SIGMA/W for a distributed load over a transverse isotropic medium (E_h^u/E_v^u=2).

5.3.2 Point Load Transient Pressure Analysis

Once the heavy equipment is in a loading position, the induced pore pressures will begin to dissipate with time with larger pore pressures immediately beneath the loaded area migrating towards the monitoring point within the grouted borehole. The rate of this pore pressure transient is dependent upon the hydraulic properties of the formation and grout.

From the pore pressure distribution, illustrated in Figure 5-12, a spatial-function was input as the initial conditions for a two-dimensional, axisymmetric SEEP/W model. The model extended 100 m radially (x-direction) and was 50 m deep (y-direction). The far-field and deepest-boundary of the model were set as zero-pressure boundaries. The same initial pore pressure distribution was subtracted from simulated pressures after 1.5 hours of dissipation, to simulate unloading. Two formation hydraulic conductivities were considered in the model, 10^{-9} and 10^{-10} m/s. The transient response of point loading simulation did not consider the presence of a borehole. The transient results show that an initial rise in pressure could be observed as excess pressures dissipate (Figure 5-13). It is also apparent that when the load is removed pore pressures will drop slightly below static levels. The transient observed during each observed loading interval (Figure 4-5) is most likely due an equalization between the grouted annulus and formation, as opposed to a dissipation of excess pressure from loading.

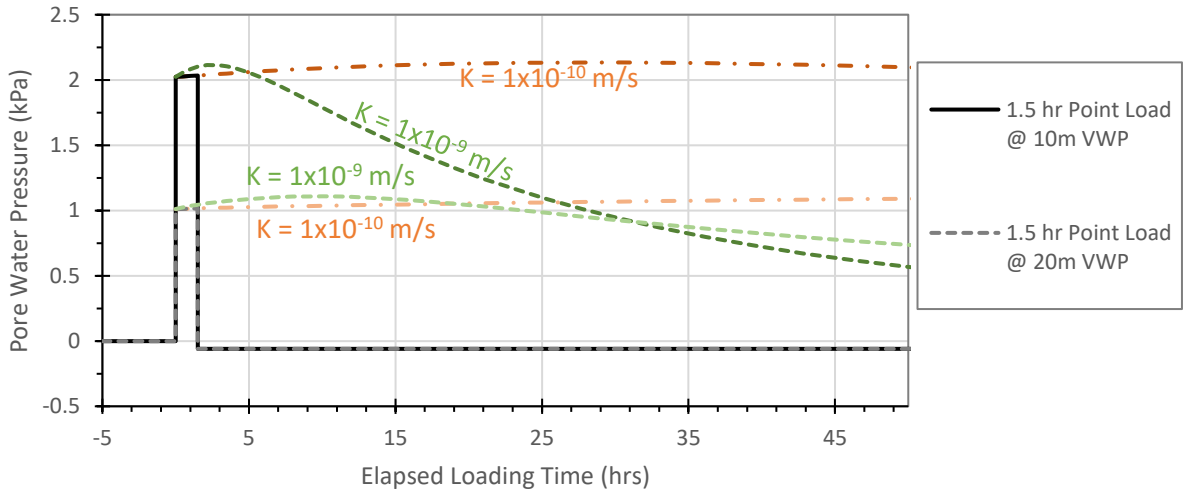

Figure 5-13 - Transient response of point loading shown at 10 and 20 m depths evaluated 5.5m away from the loading centroid. Coloured lines illustrate the pressure response if the load was left in place for 48 hours.

Considering the transient pressure response of both the point load pressure dissipation and the borehole equalization would require a fully three-dimensional model, which is beyond the scope of this project. Regardless, the point loading analysis illustrates how heavy equipment experimentation could potentially be analyzed to determine *in situ* hydraulic properties of low-permeability formations.

6.0 CONCLUSIONS AND RECOMMENDATIONS

This experiment was a fundamental study of the mechanisms which control the Barometric response Function (BRF) of a fully-grouted borehole installed in a thick aquitard. Previous research into characterizing *in situ* properties of thick clay sequences had determined that a loading efficiency can be determined through a visual-inspection method. Numerical simulations of pore pressure recovery following fully-grouted borehole installation can inversely infer hydraulic conductivity of a low-permeability formation. Barometric response functions can be used to glean additional hydrogeological information from a site.

BRFs were produced from barometric and pore pressure data, collected simultaneously. A unique BRF was determined for each of the twenty VWPs at the research site. Three distinguishing features can characterize the BRFs: the instantaneous pressure response; loading efficiency, and time-lag for equilibration. Loading efficiencies (LE) determined from the barometric response functions were similar to estimates from a visual-inspection-method. Visualizing the depth profile of loading efficiency indicated that depth (and overburden stress) was inversely proportional to compressibility. These findings are consistent with previously conducted research. There does appear to be a difference in BRFs between the continuously cored borehole and mud rotary borehole. Such differences could be attributed to the build-up of a mud filter cake or deficiencies grout backfill.

Grout samples were formed in a laboratory setting and tested to determine acoustic wave velocities. Shear and compression wave speeds can be used to determine ‘dynamic' small strain moduli. Compressibility estimates from laboratory testing and barometric loading can together help form a modulus degradation curve. According to this research, the small strain grout compressibility is approximately $1x10^{-7}$ kPa^{-1}, as compared to 4.8 x 10 -5 kPa-1from oedometer testing. This difference in grout compressibility is exemplified in transient simulations to determine formation hydraulic conductivity. Using the stiffer grout in simulations results in a formation hydraulic conductivity two-orders-of-magnitude lower than the compressible grout.

Vibrating-wire piezometers measured pore pressure changes that were resultant from heavy equipment placed near the piezometers. The magnitude of response can be estimated by the

Boussinesq solution. Transient pore pressures are similar to the barometric response function; both appear to be influenced by a compressible layer surrounding the borehole.

Future Work

The evolution of *in situ* stress, strain, flow, and material properties around a hole in the ground remains an essential problem in the various disciplines of geological engineering. Application of the instantaneous-BRF methodology outlined in this thesis could add value to existing projects and datasets. For example, researchers have recently studied changes in LE over time (David et al., 2017). They deduced that altered compressibility could impact flows near an advancing mine.

Although the analysis in this thesis considered grouted-in piezometers, improved estimates of LE can be applied to standpipes by implementing a packer system (Cook et al., 2017). The impacts of overlying or underlying aquifers can also be considered for improved hydrogeological characterization (Anochikwa et al., 2012). Correcting pore pressures by adequately considering the BRF will result in smoother groundwater level records. Proper barometric compensation allows for other phenomena to be identified more accurately than by considering a single LE value. For example, the calculation of vertical gradients or changes in external stress, such as soil moisture.

Furthering BRF research will require more precise instrumentation. The precision of sensors was identified to be one limitation of this experiment. Other researchers improved resolution using the same sensors as this project by including additional data logging hardware capable of averaging multiple sensor readings (Barr et al., 2000). Sensors and installation methods capable of better resolution have been proven, but are expensive (van der Kamp & Schmidt, 1997).

The strain due to the barometric fluctuations is not measured, but rather inferred from the changing volumetric strain and pore pressure. The compressibility derived from loading efficiency methods can aid estimations of barometric strain. However, it is feasible to install strain gauges in boreholes to measure displacements from ground-surface loading. These gauges would help constrain unknowns and help advance coupled stress-strain-pressure research. A

more rigorous calculation of the enhanced damaged zone surrounding a borehole would also be valuable.

Point load experimentation could be used to better understand the behaviour and properties of low permeability porous media. This testing may theoretically be used to quantify both transverse and directional anisotropy. Improvements to the point loading experimentation would include more precise sensors and loggers to record pressure changes, quicker placement of loads into an appropriate position, longer loading duration; and use of a heavier load with a smaller footprint.

REFERENCES

Acworth, R. I., Halloran, L. J. S., Rau, G. C., Cuthbert, M. O., & Bernardi, T. L. (2016). An objective frequency domain method for quantifying confined aquifer compressible storage using Earth and atmospheric tides. *Geophysical Research Letters*, *43*(22), 11,671-11,678. http://doi.org/10.1002/2016GL071328

Anochikwa, C. I., van der Kamp, G., & Barbour, S. L. (2012). Interpreting pore-water pressure changes induced by water table fluctuations and mechanical loading due to soil moisture changes. *Canadian Geotechnical Journal*, *49*, 357–366. http://doi.org/10.1139/t11-106

ASTM, S. D.-05. (2005). Standard Test Method for Laboratory Determination of Pulse Velocities and Ultrasonic Elastic Constants of Rock. *Astm*, *i*, 5–11. http://doi.org/10.1520/D2845-08.2

Barbour, S. L., Hendry, M. J., & Wassenaar, L. I. (2012). In situ experiment to determine advective-diffusive controls on solute transport in a clay-rich aquitard. *Journal of Contaminant Hydrology*, *131*(1–4), 79–88. http://doi.org/10.1016/j.jconhyd.2011.12.002

Barr, A. G., van der Kamp, G., Schmidt, R., & Black, T. A. (2000). Monitoring the moisture balance of a boreal aspen forest using a deep groundwater piezometer. *Agricultural and Forest Meteorology*, *102*(1), 13–24. http://doi.org/10.1016/S0168-1923(00)00094-0

Biot, M. A. (1941). General Theory of Three-Dimensional Consolidation. *Journal of Applied Physics*, *12*(2), 155. http://doi.org/10.1063/1.1712886

Bishop, A. W. (1954). The Use of Pore pressure Coefficients in Practice. *Géotechnique*, *4*(4), 148–152. http://doi.org/10.1680/geot.1954.4.4.148

Bishop, A. W. (1976). The influence of system compressibility on the observed pore pressure response to an undrained change in stress in saturated rock. *Géotechnique*, *26*(2), 371–375. http://doi.org/10.1680/geot.1976.26.2.371

Burbey, T. J. (2010). Fracture characterization using Earth tide analysis. *Journal of Hydrology*, *380*(3–4), 237–246. http://doi.org/10.1016/j.jhydrol.2009.10.037

Burland, J. B. (1989). Ninth Laurits Bjerrum Memorial Lecture: “Small is beautiful”—the

stiffness of soils at small strains. *Canadian Geotechnical Journal*, *26*(4), 499–516. http://doi.org/10.1139/t89-064

Butler, J. J., Jin, W., Mohammed, G. a, & Reboulet, E. C. (2011). New insights from well responses to fluctuations in barometric pressure. *Ground Water*, *49*(4), 525–33. http://doi.org/10.1111/j.1745-6584.2010.00768.x

Carr, B. J. (2010). Compressional and Shear Wave Seismic Studies in the Williston Basin of Central Saskatchewan, 47–56.

Caterpillar. (2017). D8T: Track-Type Tractor.

Christiansen, E. A. (1992). Pleistocene stratigraphy of the Saskatoon area , Saskatchewan , Canada: an update. *Canadian Geotechnical Journal*, (29), 1767–1778.

Clayton, C. R. I. (2011). Stiffness at small strain: research and practice. *Géotechnique*, *61*(1), 5–37. http://doi.org/10.1680/geot.2011.61.1.5

Contreras, I. a., Grosser, A. T., Ver Strate, R. H., & Strate, R. H. (2008). The use of the fully-grouted method for piezometer installation Part 1 and Part 2. *Geotechnical Instrumentation News*, *26*(2), 30–37. Retrieved from http://dx.doi.org/10.1061/40940(307)67

Cook, S. B., Timms, W. A., Kelly, B. F. J., & Barbour, S. L. (2017). Improved barometric and loading efficiency estimates using packers in monitoring wells. *Hydrogeology Journal*, *25*(5), 1451–1463. http://doi.org/10.1007/s10040-017-1537-9

David, K., Timms, W. A., Barbour, S. L., & Mitra, R. (2017). Tracking changes in the specific storage of overburden rock during longwall coal mining. *Journal of Hydrology*, *553*, 304–320. http://doi.org/10.1016/j.jhydrol.2017.07.057

Davis, D. R., & Rasmussen, T. C. (1993). A comparison of linear regression with Clark's Method for estimating barometric efficiency of confined aquifers. *Water Resources Research*, *29*(6), 1849–1854. http://doi.org/10.1029/93WR00560

Gercek, H. (2007). Poisson's ratio values for rocks. *International Journal of Rock Mechanics and Mining Sciences*, *44*(1), 1–13. http://doi.org/10.1016/j.ijrmms.2006.04.011

Gibson, R. E. (1963). An Analysis of System Flexibility and its Effect on Time-Lag in Pore-

Water Pressure Measurements. *Géotechnique*, *13*, 1–11. http://doi.org/10.1680/geot.1963.13.1.1

Hendry, M. J., Barbour, S. L., Novakowski, K., & Wassenaar, L. I. (2013). Paleohydrogeology of the Cretaceous sediments of the Williston Basin using stable isotopes of water. *Water Resources Research*, *49*(8), 4580–4592. http://doi.org/10.1002/wrcr.20321

Hendry Geosciences Inc. (2014). *Interim Letter Report II - Update of Findings to determine Hydrogeological Properties using shut in pressure transducers installed from 2012-2014*.

Hsieh, P. A. (1996). Deformation-Induced Changes in Hydraulic Head During Ground-Water Withdrawal. *Ground Water*, *34*(6), 1082–1089. http://doi.org/10.1111/j.1745-6584.1996.tb02174.x

Jacob, C. E. (1939). Fluctuations in artesian pressure produced by passing railroad-trains as shown in a well on Long Island, New York. *Transactions, American Geophysical Union*, *20*(4), 666. http://doi.org/10.1029/TR020i004p00666

Jacob, C. E. (1940). On the flow of water in an elastic artesian aquifer. *Transactions, American Geophysical Union*, *21*(2), 574. http://doi.org/10.1029/TR021i002p00574

Keller, C. K., Van Der Kamp, G., & Cherry, J. A. (1989). A multiscale study of the permeability of a thick clayey till. *Water Resources Research*, *25*(11), 2299–2317. http://doi.org/10.1029/WR025i011p02299

Kelln, C., Sharma, J., Hughes, D., & Graham, J. (2008). An improved elastic–viscoplastic soil model. *Canadian Geotechnical Journal*, *45*(10), 1356–1376. http://doi.org/10.1139/T08-057

Kirkby, W., & Pickett, P. E. (2006). *Geotechnical Manual*. *Texas Department of Transportation*.

Marefat, V., Duhaime, F., & Chapuis, R. P. (2015). Pore pressure response to barometric pressure change in Champlain clay: Prediction of the clay elastic properties. *Engineering Geology*, *198*, 16–29. http://doi.org/10.1016/j.enggeo.2015.09.005

Mikkelsen, P. E. (2002). Cement-Bentonite Grout Backfill for Borehole Instruments. *Geotechnical News*.

Moench, a F., & Hsieh, P. a. (1985). Comment on "Evaluation of Slug Test in Wells Containing a Finite Thickness Skin." *Water Resources Research*, *21*(9), 1459–1461.

Narasimhan, T. N. (2006). On Storage Coefficient and Vertical Strain. *Ground Water*, *44*(3), 488–491. http://doi.org/10.1111/j.1745-6584.2006.00160.x

Narasimhan, T. N., & Kanehiro, B. Y. (1980). A note on the meaning of storage coefficient. *Water Resources Research*, *16*(2), 423–429. http://doi.org/10.1029/WR016i002p00423

Naylor, D. J. (1974). Stresses in Nearly Incompressible Materials by Finite Elements with Application to the Calculation of Excess Pore Pressures. *International Journal for Numerical Methods in Engineering*, *8*(3), 443–460. http://doi.org/10.1002/nme.1620080302

Neuzil, C. E. (1986). Groundwater Flow in Low-Permeability Environments. *Water Resources Research*, *22*(8), 1163–1195. http://doi.org/10.1029/WR022i008p01163

Nur, A., & Byerlee, J. D. (1971). An exact effective stress law for elastic deformation of rock with fluids. *Journal of Geophysical Research*, *76*(26), 6414–6419. http://doi.org/10.1029/JB076i026p06414

Rasmussen, T. C., & Crawford, L. A. (1997). Identifying and Removing Barometric Pressure Effects in Confined and Unconfined Aquifers. *Ground Water*, *35*(3), 502–511. http://doi.org/10.1111/j.1745-6584.1997.tb00111.x

Rice, James R.; Cleary, M. P. (1976). Some Basic StressDiffusion Solutions for Fluid-Saturated Elastic Porous M Constituents. *Reviews of Geophysics and Space Physics*, *14*(2), 227–241.

Rojstaczer, S. (1988). Determination of fluid flow properties from the response of water levels in wells to atmospheric loading. *Water Resources Research*, *24*(11), 1927. http://doi.org/10.1029/WR024i011p01927

Rojstaczer, S., & Agnew, D. C. (1989). The Influence of Formation Material Properties on the Response of Water Levels in Wells to Earth Tides and Atmospheric Loading + apl • ij, *94*, 403–411.

Rudolph, D. L., & Frind, E. O. (1991). Hydraulic response of highly compressible aquitards during consolidation. *Water Resources Research*, *27*(1), 17–30.

http://doi.org/10.1029/90WR01700

Shaw, R. J., & Hendry, M. J. (1998). Hydrogeology of a thick clay till and Cretaceous clay sequence, Saskatchewan, Canada. *Canadian Geotechnical Journal, 35*(6), 1041–1052. http://doi.org/10.1139/cgj-35-6-1041

Simeoni, L. (2012). Laboratory tests for measuring the time-lag of fully grouted piezometers. *Journal of Hydrology*, *438–439*, 215–222. http://doi.org/10.1016/j.jhydrol.2012.03.025

Skempton, a. W. (1954). The Pore pressure Coefficients A and B. *Géotechnique, 4*(4), 143–147. http://doi.org/10.1680/geot.1954.4.4.143

Smerdon, B. D., Smith, L. A., Harrington, G. A., Gardner, W. P., Delle Piane, C., & Sarout, J. (2014). Estimating the hydraulic properties of an aquitard from in situ pore pressure measurements. *Hydrogeology Journal*, 1–13. http://doi.org/10.1007/s10040-014-1161-x

Smith, D. L. O., & Dickson, J. W. (1990). Contributions of vehicle weight and ground pressure to soil compaction. *Journal of Agricultural Engineering Research*, *46*(C), 13–29. http://doi.org/10.1016/S0021-8634(05)80110-6

Smith, L. A., Barbour, S. L., Hendry, M. J., Novakowski, K., & van der Kamp, G. (2016). A multiscale spproach to determine hydraulic conductivity in thick claystone aquitards using field, laboratory, and numerical modeling methods. *Water Resources Research*, *52*, 1–20. http://doi.org/10.1002/2014WR015716

Smith, L. A., van der Kamp, G., & Hendry, M. J. (2013). A new technique for obtaining high-resolution pore pressure records in thick claystone aquitards and its use to determine in situ compressibility. *Water Resources Research*, *49*, 732–743. http://doi.org/10.1002/wrcr.20084

SNC-Lavalin Inc. (2014). *2014 Weyburn Coring and Instrumentation Program*. Saskatoon, Saskatchewan.

Spane, F. A. (2002). Considering barometric pressure in groundwater flow investigations. *Water Resources Research, 38*(6), 14-1-18. http://doi.org/10.1029/2001WR000701

Terzaghi, K. (1927). Principles of final soil classification. American Society of Civil Engineers.

Toll, N. J., & Rasmussen, T. C. (2007). Removal of barometric pressure effects and earth tides from observed water levels. *Ground Water*, *45*(1), 101–105. http://doi.org/10.1111/j.1745-6584.2006.00254.x

van der Kamp, G. (2001). Methods for determining the in situ hydraulic conductivity of shallow aquitards - An overview. *Hydrogeology Journal*, *9*(1), 5–16. http://doi.org/10.1007/s100400000118

van der Kamp, G., & Gale, J. E. (1983). Theory of earth tide and barometric effects in porous formations with compressible grains. *Water Resources Research*, *19*(2), 538–544. http://doi.org/10.1029/WR019i002p00538

van der Kamp, G., & Maathuis, H. (1991). Annual fluctuations of groundwater levels as a result of loading by surface moisture. *Journal of Hydrology*, *127*(1–4), 137–152. http://doi.org/10.1016/0022-1694(91)90112-U

van der Kamp, G., & Schmidt, R. (1997). Monitoring of total soil moisture on a scale of hectares using groundwater piezometers. *Geophysical Research Letters*, *24*(6), 719–722. http://doi.org/10.1029/97GL00521

Vaughan, P. R. (1969). A Note on Sealing Piezometers in Boreholes. *Géotechnique*, *19*(3), 405–413. http://doi.org/10.1680/geot.1969.19.3.405

APPENDICES

Appendix A - Grout One-Dimensional Consolidation (Oedometer) Results

(Smith et al., 2013) conducted oedometer testing on grout samples to determine the one-dimensional compressibility, which is required for the calculation of specific storage. Raw data from the test are included in Figure A-1.

MDH ENGINEERED SOLUTIONS

One-Dimensional Consolidation Test - ASTM D 2435

Project No:	L2981	Project Name	-
Date:	03-Aug-11	Tech:	TH
Sample No:	Grout B#32	Checked by:	JG
Test Procedure:	Trimmed from core specimen		
Method of testing:	Method B	Condition of test:	inundated

Input:

Diameter of ring:	63.72	mm
Height of sample:	19.49	mm
Specific gravity:	2.70	assumed
Initial wet sample mass:	100.18	g
Initial water content:	41.3	%
Initial LVDT reading:	6.3440	mm
Mechanical Advantage:	11.00	

Calculations:

Cross-sectional area:	31.89	cm^2	3.2E-03 m^2
Total volume:	62.15	cc (prior to loading)	
Dry mass of solids:	70.90		
Volume of solids:	26.26	cc	3.0E-07 m^3
Volume of voids:	35.89	cc (prior to loading)	
Initial void ratio:	1.37	(prior to loading)	
Initial deg. of saturation	0.8158		
Initial wet density:	1612	kg/m^3 (prior to loading)	
Initial dry density:	1141	kg/m^3 (prior to loading)	

		At End of Primary Consolidation							Coefficient of Consolidation						
Loading Increment	Pressure (kPa)	R_{150} (mm)	Uncorrected Sample Height (mm)	Equipment Compressibility (mm)	Corrected Sample Height (mm)	Volume of Sample (cc)	Volume of Voids (cc)	Void Ratio	Average Void Ratio	R_{50} (mm)	Corrected Sample Height at R_{50} (mm)	H_{t50} (mm)	time50 (sec)	Coefficient of Consolidation c_v (cm^2/s)	coefficient of compressibility a_v (per kPa)
swelling	10.6							1.37							
1	21.8	6.3360	19.4820	0.0000	19.4820	62.13	35.87	1.37	1.37	6.34	19.48	9.74	10200	1.83E-05	
2	44.1	6.3280	19.4740	0.0080	19.4820	62.13	35.87	1.37	1.37	6.33	19.48	9.74	12000	1.56E-05	
3	85.8	6.3260	19.4720	0.0180	19.4900	62.15	35.89	1.37	1.37	6.33	19.49	9.75	12600	1.48E-05	
4	170.4	6.2860	19.4320	0.0320	19.4640	62.07	35.81	1.36	1.37	6.30	19.47	9.74	4080	4.58E-05	3.73E-05
5	339.6	6.1840	19.3300	0.0480	19.3780	61.79	35.54	1.35	1.36	6.20	19.40	9.70	3720	4.98E-05	6.17E-05
6	680.8	6.1220	19.2680	0.0740	19.3420	61.68	35.42	1.35	1.35	6.13	19.35	9.68	960	1.92E-04	1.28E-05
7	1357.6	6.0620	19.2080	0.1060	19.3140	61.59	35.33	1.35	1.35	6.07	19.32	9.66	10800	1.70E-05	5.02E-06
8	2703.0	5.9860	19.1320	0.1460	19.2780	61.48	35.22	1.34	1.34	6.00	19.29	9.65	10800	1.70E-05	3.25E-06
9	5026.4	5.8945	19.0405	0.2000	19.2405	61.36	35.10	1.34	1.34	6.00	19.34	9.67	10800	1.71E-05	1.96E-06
10	1357.6	5.9880	19.1340	0.1260	19.2600	61.42	35.16	1.34	1.34						
11	339.6	6.0600	19.2060	0.0760	19.2820	61.49	35.23	1.34	1.34						
12	85.8	6.0960	19.2420	0.0460	19.2880	61.51	35.25	1.34	1.34						
13	10.6	6.1210	19.2670	0.0240	19.2910	61.52	35.26	1.34	1.34						

Figure A-1 - One-Dimensional Consolidation Results on Grout Samples

The hydraulic conductivity inferred from oedometer testing was calculated using Equation A-17. Grout properties at varying confining stresses, estimated from oedometer testing, are presented in **Table A-**1.

$$K_{cv} = m_v c_v \rho_w g \quad \text{(A-1)}$$

Where Kcv is the hydraulic conductivity from oedometer testing (m/s), c_v is the coefficient of consolidation (m^2/s), $p_w g$ is the specific gravity of water.

Table A-1 – Grout parameters determined from one-dimensional consolidation testing

Confining Stress (kPa)	Equivalent Depth* (m)	c_v (m^2/s)	m_v ($1/kPa^{-1}$)	K_{cv} (m/s)
170.4	13.1	4.6×10^{-9}	3.7×10^{-5}	1.7×10^{-9}
339.6	26.1	5.0×10^{-9}	6.2×10^{-5}	3.0×10^{-9}
680.8	52.4	1.9×10^{-8}	1.3×10^{-5}	2.4×10^{-9}
1357.6	104.4	1.7×10^{-9}	5.0×10^{-5}	8.4×10^{-10}
2703	207.9	1.7×10^{-9}	3.3×10^{-6}	5.4×10^{-11}
5026.4	386.6	1.7×10^{-9}	2.0×10^{-6}	3.3×10^{-11}

***Note -** Assuming hydrostatic conditions with a water table at 3mbgs and saturated unit weight of 20 kN/m*

Appendix B - Additional BRF Deconvolution Details

Barometric response functions had been calculated on six data sets collected at different times. The results from data collected are summarized in Table B-1 and Table B-2.

Weighting was found to influence BRF results. Although a weighted-average could compensate for noise and visualize a smoother pore pressure record, if this weighting is applied before BRF analysis, it would influence the results. The long-term loading efficiency is much less influenced by weighting than the instantaneous response. It is therefore better to apply the BRF deconvolution to a longer data set

Table B-1 – Instantaneous Pressure Response determined from BRF deconvolution

Depth (m)	Instantaneous BRF Response (-)						
	1	2	3	4	5	6	Average (Data Set 2 to 5)
10	0.19	0.38	0.46	0.44	0.29	0.39	0.39
20	0.47	0.66	0.63	0.63	-	0.48	0.64
30	0.43	0.70	0.61	0.59	0.31	0.34	0.55
40	0.45	0.69	0.63	0.68	-	0.27	0.67
50	0.48	0.52	0.49	0.52	0.42	1.05	0.49
60	0.48	0.60	0.49	0.40	-	0.25	0.50
70	0.50	0.73	0.63	0.78	0.33	-0.05	0.62
80	0.17	0.67	0.69	0.38	-	0.02	0.58
90	0.36	0.67	0.31	0.46	0.24	0.31	0.42
100	-0.21	0.13	0.11	0.21	-	1.27	0.15
110	0.42	0.51	0.77	0.68	0.25	0.70	0.55
120	0.03	-0.05	0.22	0.24	-	-0.41	0.14
130	0.78	0.32	0.90	0.65	0.37	-0.12	0.56
140	-0.01	0.26	0.29	-0.38	-	0.11	0.05
150	0.05	0.59	-0.09	0.43	0.29	0.12	0.30
160	0.36	0.13	0.06	0.12	-	-0.16	0.11
170	-0.05	0.50	0.64	0.53	0.16	0.63	0.45
180	-0.54	-0.08	-0.18	0.15	-	-0.22	-0.04
190	0.81	-0.02	1.18	0.69	0.10	-1.42	0.49
200	1.12	0.03	-0.01	0.22	-	0.92	0.08

Table B-2 - Loading Efficiency Determined from BRF Deconvolution

Depth (m)	BRF Loading Efficiency (-)						
	1	2	3	4	5	6	Average (Data Set 2 to 5)
10	0.70	0.69	0.75	0.75	0.79	0.67	0.74
20	0.85	0.87	0.89	0.87	-	0.75	0.88
30	0.95	0.95	0.93	0.95	0.89	0.82	0.93
40	0.92	0.98	0.96	0.99	-	0.83	0.98
50	0.92	0.91	0.81	0.89	0.86	0.78	0.87
60	0.92	0.90	0.88	0.90	-	0.67	0.89
70	0.94	0.86	0.88	0.78	0.90	0.78	0.85
80	0.64	0.76	0.81	0.75	-	0.79	0.77
90	0.99	0.79	0.71	0.87	0.79	0.41	0.79
100	0.05	0.24	0.28	0.38	-	0.64	0.30
110	1.10	0.70	0.62	0.80	0.73	0.55	0.71
120	0.17	0.10	0.21	0.14	-	0.24	0.15
130	1.23	0.66	0.78	0.74	0.73	0.80	0.73
140	0.16	0.05	0.02	0.02	-	0.27	0.03
150	1.11	0.70	0.68	0.64	0.68	0.37	0.67
160	-0.01	0.10	0.14	0.17	-	-0.12	0.14
170	1.17	0.73	0.72	0.66	0.69	0.98	0.70
180	0.39	0.15	0.11	0.03	-	0.25	0.10
190	1.06	0.55	0.79	0.76	0.74	0.85	0.71
200	0.33	0.19	0.50	0.39	-	1.26	0.36